Phase Change Heat Transfer on Micro/Nano Structured Enhanced Surfaces

by
Ahmad Reza Motezakker

Submitted to the Graduate School of Natural Science and Engineering

In partial fulfillment of the requirement for the degree of

Master of Science

Sabanci University

July 2018

Phase-change Heat Transfer using Micro/Nano Scale Enhanced Surfaces

APPROVED BY:

Prof. Dr. Ali Kosar
(Thesis Supervisor)

Assoc. Prof. Dr. Burc Misirlioglu

Asst. Prof. Dr. Yegan Erdem
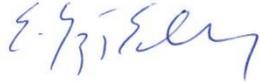
DATE OF APPROVAL: 20/07/2018

ABSTRACT

Phase Change Heat Transfer on Micro/Nano Structured Enhanced Surfaces

Ahmad Reza Motezakker

Master Dissertation, July 2018

Supervisor: Prof. Dr. Ali Kosar

Key words: Cooling Systems, Phase change, Pool boiling, Micro/Nano structures, Bio-coating, Biphilic

Due to the recent trend of miniaturization of electronic devices, thermal management has become obligatory and yet challenging. There are many cooling methods such as spray cooling and passive cooling techniques involving phase change phenomena. Among phase change (liquid-vapor) phenomena, boiling is a widely used phenomenon in the industry. Owing to a large amount of heat dissipation and achievable high heat transfer coefficients, it is one of the most effective heat transfer mechanisms for cooling high power microelectronic devices. With the help of material science and nanotechnology, various types of nanostructures on surfaces are now available. Different types of enhanced surfaces (e.g. micro/nano structured surfaces) have been used by many investigators to enhance heat transfer coefficient and also reduce wall superheat. In this thesis, two different futuristic types of enhanced surfaces have been designed, fabricated and implemented. First, an effective and facile method for surface enhancement via crenarchaeon *Sulfolobus Solfataricus* P2 bio-coatings is presented and tested under boiling condition. Additionally, enhanced surfaces with mixed wettability (Biphilic surfaces) have been designed and fabricated to assess the effect of heterogeneous wettability on boiling heat transfer and cooling performance. In both cases, high heat removal performance has been achieved. Promising results for both

types of coatings suggest such coatings as a novel solution for high efficiency and enhanced cooling applications.

ÖZET

Mikro / Nano Yapılandırılmış ve Geliştirilmiş Yüzeylerde Faz Değişimi Isı Transferi

Ahmad Reza Motezakker

Master Dissertation, Temmuz 2018

Danışman: Prof. Dr. Ali Kosar

Son zamanlarda elektronik cihazların minyatürleştirilmesi eğilimi nedeniyle, termal yönetim zorunlu ve zorlu hale gelmiştir. Faz değişimi fenomeni içeren sprey soğutma ve pasif soğutma teknikleri gibi birçok soğutma yöntemi vardır. Faz değişimi (sıvı-buhar) fenomenleri arasında, kaynatma, endüstride yaygın kullanılan bir fenomendir. Yanı sıra, yüksek miktarda ısı kaybı ve ulaşılabilir yüksek ısı transfer katsayıları nedeniyle, yüksek güçlü mikroelektronik cihazların soğutması için en etkili ısı transfer mekanizmalarından biridir. Malzeme bilimi ve nanoteknoloji yardımıyla, yüzeylerdeki çeşitli nano yapılar mevcuttur. Isı transfer katsayısını arttırmak ve aynı zamanda duvar süper ısısını azaltmak için, farklı geliştirilmiş yüzeyler (örneğin mikro / nano yapılı yüzeyler) birçok araştırmacı tarafından kullanılmıştır. Bu tezde iki farklı fütüristik geliştirilmiş yüzey türü tasarlanmış, imal edilmiş ve uygulanmıştır. Birincisi, crenarchaeon Sulfolobus Solfataricus P2 bio-kaplamaları ile yüzey iyileştirme için etkili ve kolay bir yöntem sunulmakta ve kaynatma koşulu altında test edilmektedir. Ek olarak, karışık ıslanabilirlik (Bifilik yüzeyler) ile geliştirilmiş yüzeyler, heterojen ıslanabilirliğin kaynama ısı transferi ve soğutma performansı üzerindeki etkisini değerlendirmek üzere tasarlanmış ve imal edilmiştir. Her iki durumda da, yüksek ısı giderme performansı elde edilmiştir. Her iki kaplama türü için umut verici sonuçlar, yüksek verimlilik ve geliştirilmiş soğutma uygulamaları için yeni bir çözüm olarak bu tür kaplamaları önermektedir.

To my family members…

Acknowledgments

I would like to thank:

- Professor Ali Koşar, my MSc program advisor, for offering me this great opportunity to learn and experience the exciting realm of boiling. His unconditional support, encouragement and guidance helped me to accomplish my research objectives. His personality, knowledge and achievements have been always inspiring for me.

- Professor Guillermo Villanueva, for hosting me at the Ecole Polytechnique Federale de Lausanne (EPFL) during summer 2017 to have access to Center of MicroNanoTechnology (CMI) for fulfilling a part of my MSc program related to fabrication of Biphilic enhanced surfaces.

- Professor Burç Mısırlıoğlu and Professor Yegan Erdem, my thesis jury members, for their dedication and constructive comments for improving the technical context of the thesis.

- My colleagues at Micro-Nano Scale Heat Transfer and Microfluidic Research Group at Sabanci University, especially Abdolali Khalili Sadaghiani, who guided me in boiling topic and conducting reliable experimental studies; Mehrdad Karimzadehkhouei, for helping me with the thesis format and encouraging me during difficulties of my MSc study.

- Dr. Tom Larsen, postdoc researcher of Advanced Nano-electromechanical Systems Laboratory (ANEMS) at EPFL, for his precious recomendations related to both academic and personnal issues.

- Yunus Akkoc, Ph.D. candidate of Molecular Biology Genetics and Bioengineering program at Sabanci University, for his exemplary and high-quality efforts in preparing the bio-coating samples.

- Scientific and Technological Research Council of Turkey (TUBITAK) and Sabanci University for supporting me during my MSc study.

- Sabanci University (SU), Faculty of Engineering and Natural Science (FENS), and Sabanci University Nanotechnology Research and

Application center (SUNUM) and staff for providing excelent research equipment and environment.

- My friends, who were always there for me.
- My lovely family for their unconditional love, support, and simply everything. Without them, this journey would not be possible for me.

Table of Contents

List of Tables

List of Figures

CHAPTER 1: Introduction

Heat transfer has three main mechanisms; including radiation, conduction and convection. In radiation, heat transfer takes place in form of electromagnetic waves. Conduction is perhaps the most regular heat transfer mechanism in nature, which happens via molecules within the material particles of material as a result of temperature gradients. In convection, heat transfer occurs as a result of bulk fluid motion and conduction inside the fluid.

Due to its nature and capability, convective heat transfer is widely used in various applications in industry such as in cooling and heating applications. Free convection, forced convection and phase change convection are three classifications of convective heat transfer. Among them, convective heat transfer with phase change is more effective due to the utilization of latent heat of the fluid.

The Newton's cooling law is used to calculate the rate of convective heat transfer in a system.

$$q'' = h \ (T_s - T_f) \tag{1}$$

where q'' is the amount of heat flux (heat transfer rate per unit era), h is the coefficient of heat transfer, T_s is the surface temperature and T_f is the surrounding fluid temperature.

1-1 Boiling

Flow boiling (forced convection boiling) and pool boiling are two categories of boiling heat transfer. While, the liquid motion is due to an external force in flow boiling, in pool boiling, motion and mixing of the fluid are due to the growth and departure of nucleated bubbles in a pool during boiling. In comparison with the prevalent cooling mechanisms such as free and forced convection with liquids or gases, convection with phase change (boiling) leads to the highest heat transfer coefficient ranging from 2500 to 100000 (W/m^{2}K) [1]. Due to the implementation of latent heat, boiling heat transfer mechanism is extensively used in the systems providing high heat removal rate from small surface areas. Numerous difficulties such as providing high pressure difference

and sealing have been recorded for flow boiling. On the other hand, pool boiling system is simple with relatively high heat removal rate.

1-2 Pool Boiling

In pool boiling, the pool of saturated working fluid is located on top of the heating part. Boiling heat transfer takes place on the surface of submerged heating section, which is in direct contact with the working fluid. Liquid to vapor phase change is the reason for high heat removal performance of pool boiling systems. One of the most important advantages of pool boiling systems is that there is no need to provide pressure difference for working fluid flow over the heating part, thereby representing more desirable system from economic point of view.

Due to the potential for obtaining high heat removal rates with pool boiling, many applications related to electronic cooling, power generation, refrigeration and distillation involve phase change heat transfer. As a result, many recent studies have been conducted to enhance boiling heat transfer and to reach ultra-high heat flux cooling. Changing heating surface characteristics and working fluid are two major ways, which have been used by many researchers to maximize the boiling heat transfer performance.

1-3 Boiling Curve

The boiling curve, which represents the boiling phenomenon, consists of heat flux and wall superheat (wall temperature minus the saturation temperature) on a heating surface. When a typical boiling curve is examined, there exist single phase natural and later forced convective heat transfer mechanisms prior to nucleation from the heater surface to the working liquid (Figure 1-1, point A to B). As the heat flux increases, nucleate boiling incepts, and isolated bubbles can be first seen on the heated surface (Figure 1-1, point C). In this region, the bubble departure frequency and number of active nucleation sites are dependent on the thermal boundary conditions (wall superheat, wall heat flux, surface morphology) (Figure 1-1, point C to D). In the fully developed nucleate boiling region, the rate of bubble generation increases rapidly, thereby resulting in interactions among adjacent bubbles and generating vapor columns

on the surface (Figure 1-1, point D to E). For higher wall superheat, a greater lateral coalescence of vapor columns contributes to the formation of dry spots. The maximum in the profile highlights the critical heat flux (CHF) condition (Figure 1-1, point E, corresponding to CHF). Beyond this point, high vapor generation causes a vapor blanket, which covers the surface. Consequently, the vapor blanket acts as an insulating layer and leads to a dramatic increase in the surface temperature, resulting in burn-out condition on surfaces (Figure 1-1, point E to F). Due to its dependency on many parameters, the CHF phenomenon is complex and hard to predict.
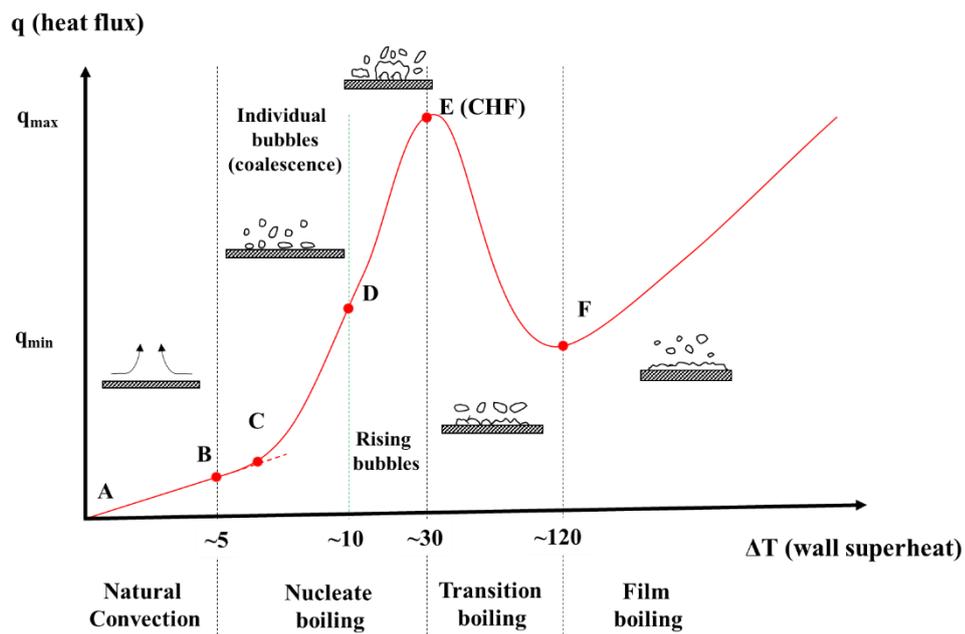
Figure 1−1 A typical boiling curve for pool boiling including natural convection, nucleate boiling, transition boiling and film boiling

In all the practical applications, critical heat flux is the endpoint of safe zone in the cooling systems. To prevent melting and failure of cooling systems, many studies have been done by many researchers to widen safe working conditions of the systems via surface enhancement and trying various working fluids such as nanofluids. Due to its dependency on many parameters, the CHF phenomenon is complex and hard to predict. For example, Kutateladze [2] and Zuber [3] proposed useful correlations for CHF, based on properties such as working fluid, gravity and system pressure.

1-4 Literature Review on Enhanced Surfaces

Due to the recent trend of miniaturization of electronic devices, thermal management of such devices has become obligatory and yet challenging. There are many cooling methods such as spray cooling [4, 5] and passive cooling techniques [6-8] involving phase change phenomena. Among phase change (liquid-vapor) phenomena, boiling is a widely used phenomenon in the industry [9]. Owing to a large amount of heat dissipation and achievable high heat transfer coefficients, it is one of the most effective heat transfer mechanisms for cooling high power microelectronic devices [10, 11]. Due to the potential for obtaining high heat removal rates with boiling phenomena, many applications related to electronic cooling, power generation, refrigeration and distillation involve phase change heat transfer[12].

During recent years, extensive experimental and numerical research has been performed to enhance pool boiling heat transfer. With the help of material science and nanotechnology, many types of nanostructures on surfaces become now available [13, 14]. Different types of enhanced surfaces (e.g. micro/nano structured surfaces) have been used by many investigators to enhance heat transfer coefficient and also reduce wall superheat. As an example, Chu et al. [15] conducted an experimental study to show the effect of structured surfaces on pool boiling heat transfer. They used microstructures with wide range of roughness to enhance critical heat flux.
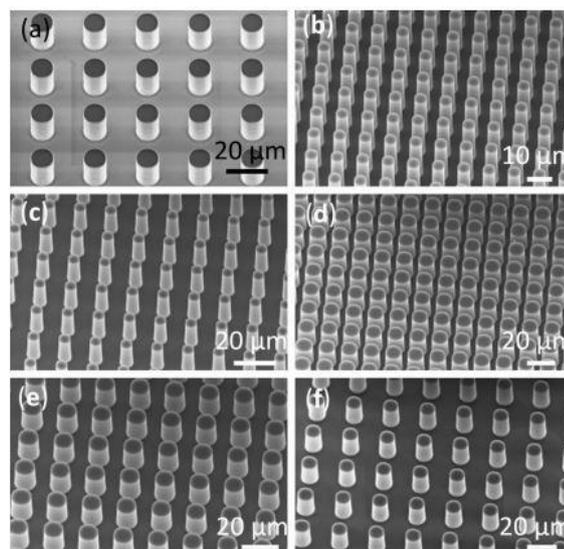
Figure 1–2 Fabricated silicon microstructures by Chu et al. [15]

Ahn et al. [16] developed a nano-structured surface using multi walled carbon nanotubes and reached 40% critical heat flux enhancement in pool boiling. These surfaces could play a role in enhancing nucleation bubble sites [17-21] or changing in wettability [22-24].
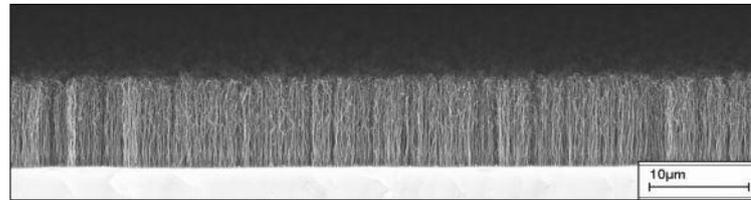
Figure 1–3 Multi walled carbon nanotubes on silicon wafer by Ahn et al. [16]

There are many studies, which analyze the bubble creation [25-27] and enhancement of pool boiling heat transfer via generating more active nucleation sites [28-31]. [32-34] using different enhanced surfaces to show their effect on pool boiling with different working fluids such as nanofluids.
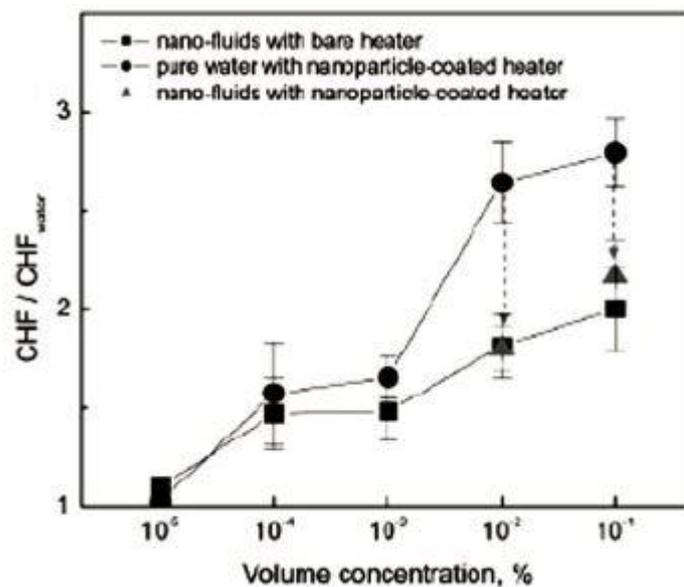
Figure 1–4 The effect of nanofluid and nano structured surfaces on CHF enhancement by Kim et al. [33]

Many of investigators have used porous surfaces to show their effects on heat transfer [35-39]. Xu et al. reported a 120% enhancement in heat transfer using a composite copper porous surface relative to the plain surface [40].
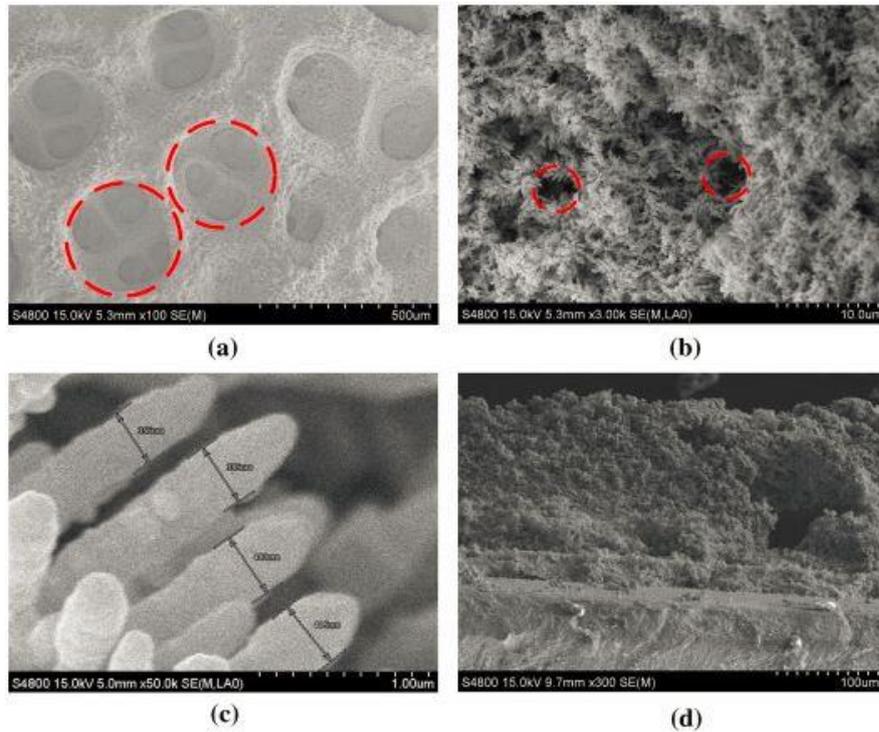
Figure 1−5 SEM images of composite porous structure for pool boiling enhancement by Xu et al. [40]

Lee et al. [41] enhanced nucleate boiling heat transfer and also achieved lower wall superheat pool boiling using nano-porous surfaces. Li et al. [42] investigated the effect of multiscale modulated porous structures on pool boiling, and three times larger heat transfer coefficients relative to the plain surface were reported.
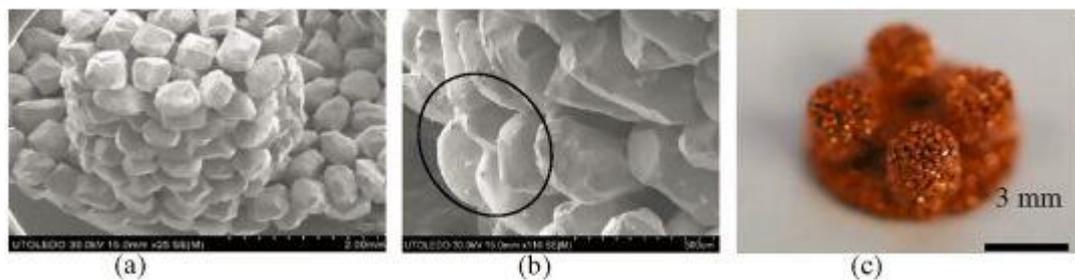
Figure 1−6 Modulated porous structures for enhancing boiling heat transfer coefficient by Li et al. [42]

Tang et al. [43] utilized metallic nanoporous surfaces, and significant enhancement in cooling and heat transfer coefficient was reported. A porous coating with reentrant cavities was developed by Deng et al. [44]. This porous coating increased the number

6

of bubble nucleation sites and prevented early condensation. Reentrant cavity makes liquid replenishment and surface rewetting much easier. Reentrant cavities are able to trap vapor during bubble nucleation; as a result, stable bubble nucleation sites were provided, which enhanced pool boiling [45].
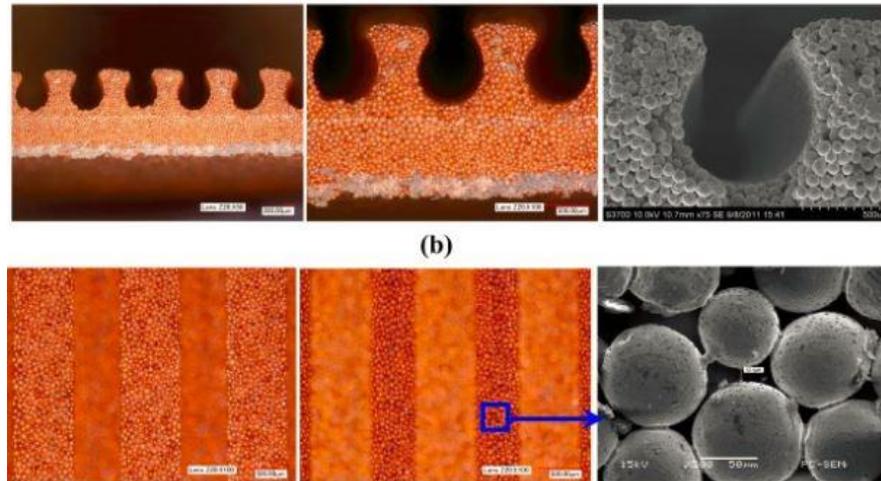
Figure 1–7 Providing stable nucleation sites by reentrant cavities [45]

Later researchers reported that nucleate boiling heat transfer and CHF are both significantly affected by surface roughness [46, 47], wettability [48, 49] and heater properties such as size and orientation[50]. There have been many studies on the enhancement of boiling heat transfer and widening the safe working conditions of thermal systems via surface modifications [15, 51, 52]. As a consequence, pool boiling heat transfer has been enhanced using micro-nano structures [53, 54], coated particles [55, 56] and nanowires [57, 58].

Recently, the effects of textured surfaces such as nanowire arrays [58, 59], porous media [60, 61] and graphene structures [62] on boiling heat transfer and CHF were investigated in the literature.
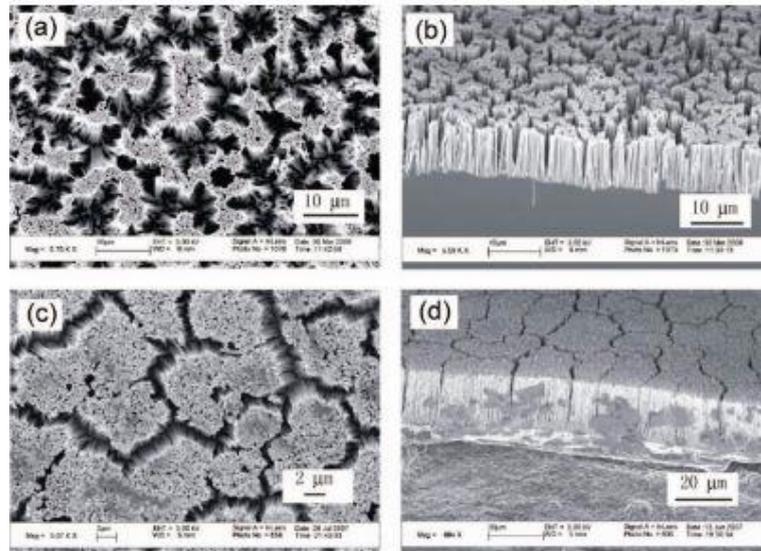
Figure 1–8 Fabricated nanowires for pool boiling enhancement [58]

Recently, thanks to its unique properties and interesting capabilities, graphene has received much attention and has been recently studied. Graphene consisting of sp^2-hybridized carbon atoms in two dimensional hexagonal lattice [63] has been a promising alternative for many fields owing to its high thermal and electrical conductivity, noteworthy optical transmittance, superior chemical stability and high flexibility [64-67]. Although graphene has these unique properties, its preparation typically results in cracks, wrinkling, defects and mechanical problems when integrated into three dimensional applications [57, 68-70]. To overcome this drawback, graphene has been prepared in three dimensional forms such as aerogel, foam and sponge during the last decade. These forms have low mass density, large surface area, good mechanical stability, high thermal and electrical conductivity. Besides energy, sensing, detecting, tissue engineering, and environmental applications [67, 71, 72], three dimensional (3D) graphene frameworks also have a potential in heat transfer enhancement because of their high thermal conductivity and porosity [73-79].
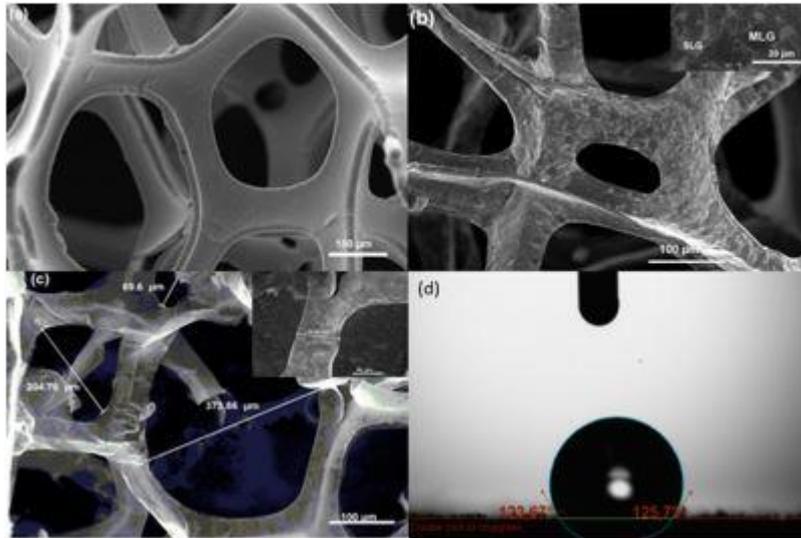
Figure 1–9 3D foamlike graphene structure for phase change cooling systems [80]

The combination of porosity and hydrophilicity provides the greatest enhancement in CHF [80]. Porous layers mostly enhance CHF by providing vapor escape paths [81, 82]. According to the reported data[83], thick porous layers do not perform well in terms of heat transfer at high heat fluxes due to higher number of dry spots.
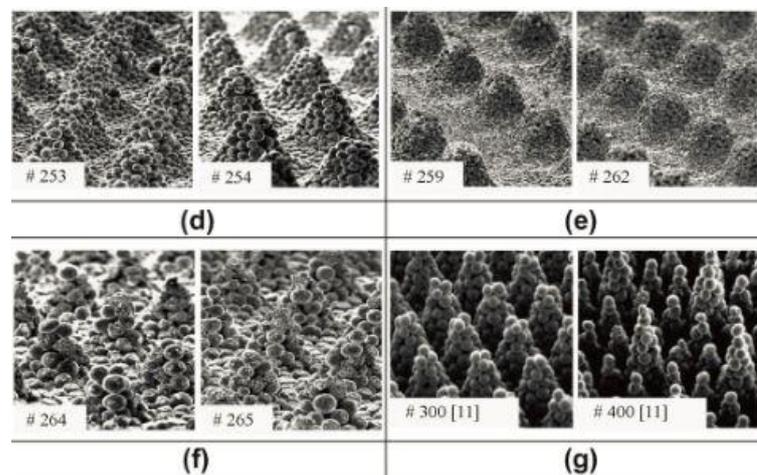
Figure 1–10 Modulated porous media for enhanced pool boiling [84]

1-5 Research Objectives

According to the literature review, heat transfer coefficient and CHF enhancement are related to surface characteristics such as morphology, wettability, roughness, and etc. The more bubble nucleation, the more heat dissipation from the heating surface, resulting in a more energy efficient cooling system.

The aim of this study is to represent novel enhanced surfaces for phase change cooling applications and assess the heat transfer mechanisms on the enhanced surfaces. To have a better understanding of the bubble nucleation and heat transfer mechanism, bubble dynamics is examined using high speed imaging in various heat fluxes.

Two different kind of enhanced surfaces have been investigated:

- Crenarchaeon *Sulfolobus solfataricus* P2 bio-coatings. The Bio-coating has been tested to accomplish following research objectives:
    - ➢ Presenting novel surface modifications via crenarchaeon *Sulfolobus solfataricus* P2.
    - ➢ Examining pool boiling heat transfer performance of such coatings at high fluxes and its durability.
    - ➢ Investigating the thickness effect of such coatings on phase change heat transfer.
- Enhanced surfaces with mixed wettability (Biphilic Surfaces). The aim of testing such enhanced surfaces is listed below:
    - ➢ Investigating the effect of biphilic surfaces on pool boiling heat transfer.
    - ➢ Presenting a facile fabrication method for fabrication of surfaces with heterogeneous wettability.
    - ➢ Offering the optimum ratio of hydrophobic to total surface area of enhanced surfaces.
    - ➢ Assessing the bubble dynamics on such enhanced surfaces various heat fluxes.
    - ➢ Analyzing the effect of biphilic surfaces on controlling the contact lines of liquid, gas and solid phases.

CHAPTER 2: Experimental Procedure and Data Reduction

2-1 Experimental setup

The schematic of the experimental setup is displayed in Figure 2-1. The glass block is a hollow cube and has outer and inner dimensions of $60{\times}60{\times}60$ and $40{\times}40{\times}40$ mm^3, respectively. The aluminium heating part has four vertical housing holes at the bottom for cartridges and five holes for T-type thermocouples. With the help of a digital power supply with high precision multimeters, current and voltage were adjusted. The power supply was connected to cartridge heaters, which were press-fitted into cylindrical holes, while high quality conductive silicon grease was utilized to fill the gap between the cartridge heaters and inner areas of the holes. Two holder plates were used to sandwich the glass block and the Teflon block. The upper holder plate has four holes, which were used to fill up the glass block with working fluid, insert a thermocouple to measure bulk temperature of fluid, insert a vertical heater to keep the fluid at saturation temperature and make a connection with the vertical condenser to provide a constant supply of deionized water. Plastic gasket sealers with resistance to high temperatures were used between glass block edges and upper plates to prevent any leakage. The reflux condenser is made of concentric glass tubes of inner and outer diameters of 22 mm and 40 mm, respectively, and a length of 40 cm. The gap between the outer and inner tubes was filled with water to condense the vapor escaping through the inner tube, which is open to atmosphere, to maintain the tests at the ambient pressure. The volume of liquid was measured before and after each test to check for the change in the liquid amount. It was found that the vertical reflux condenser was efficient, and the amount of water remained nearly the same. All the temperatures and power readings were recorded under steady state conditions. To ensure repeatability, every sample was tested three times. The heat flux was increased in small steps until the CHF point was reached. At this point, an excessive rise in wall temperature and a vapor blanket on the samples were observed. The experimental data were reduced to obtain the heat transfer coefficient and heat flux. A high-speed camera (250 frames/sec) was used to visualize pool boiling experiments. Bubble dynamics and behavior prior to and during the departure were examined and analyzed to attain a better understanding of the

enhancement mechanism. For each experiment, more than 50 bubbles were selected to determine average bubble departure volume.
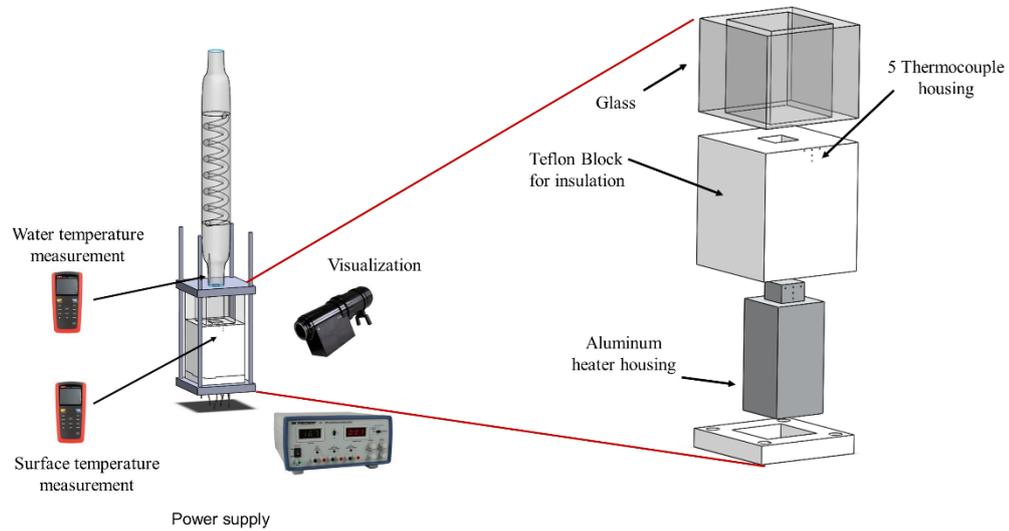
Figure 2–1 The schematic of experimental setup

2-2 Setup Calibration

The locations of the temperature measurements in the heating block are shown in Figure 2-2. Accordingly, there are five holes for thermocouples to read temperatures. The vertical temperature readings were used to obtain the vertical temperature gradient, while the horizontal temperature readings (located 1 mm beneath the sample) were used for wall temperature measurements. The surface temperature was calculated with the help of vertical measurements of T_5, T_4 and average temperature of the experimental setup right beneath the test section, $T_{ave} = (T_1 + T_2 + T_3)/3$. As can be seen in Figure 2-2, there are aluminum block, thermal paste and silicon sample between T_{ave} and surface temperature, T_s.
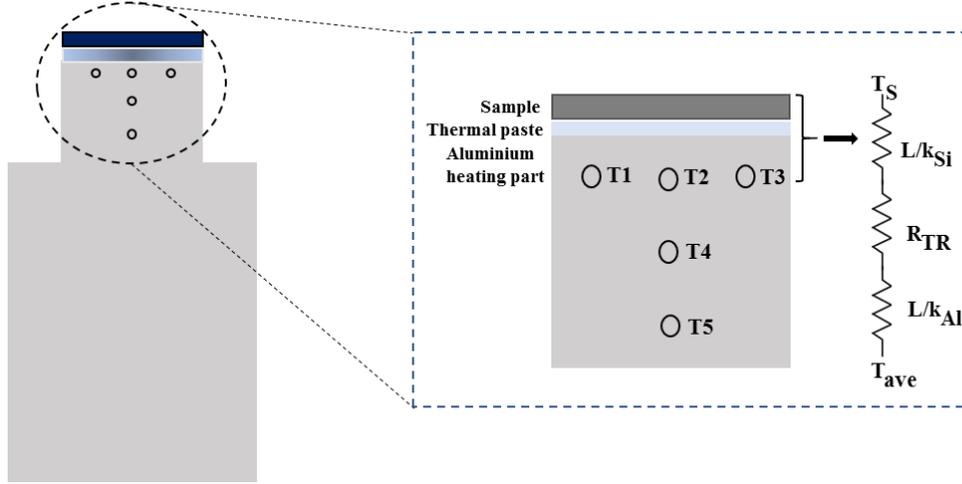
Figure 2–2 The schematic of the heated section

The surface temperatures are obtained by using the thermal contact resistance from the T_{ave} to the silicon surface with the average of the thermocouple measurements, as:

$$T_s = T_{ave} - q'' \left(\frac{L_{Al}}{K_{Al}} + R_{TR} + \frac{L_{Si}}{K_{Si}} \right) \tag{2}$$

where R_{TR} is the contact resistance of thermal paste between the aluminum and the silicon surface. The difference between saturation temperature, T_{sat}, and the surface temperature, T_s is defined as the wall superheat ΔT_{sat}.

2-3 Thermocouple Calibration

Totally, six T-type thermocouples are used in the current study in order to measure wall temperatures of test section and saturated fluid temperature. The T-type thermocouples are calibrated using a precision thermometer. The thermocouples are tied to a thermometer and submerged in a liquid bath. The bath is equipped with a temperature controller. All the temperatures related to thermocouples and thermometer were recorded. Afterwards, a linear calibration curve is drawn for each thermocouple reading with the temperature of the thermometer. Accordingly, the maximum error was 2.5%. The calibration results are presented below for all the thermocouples.
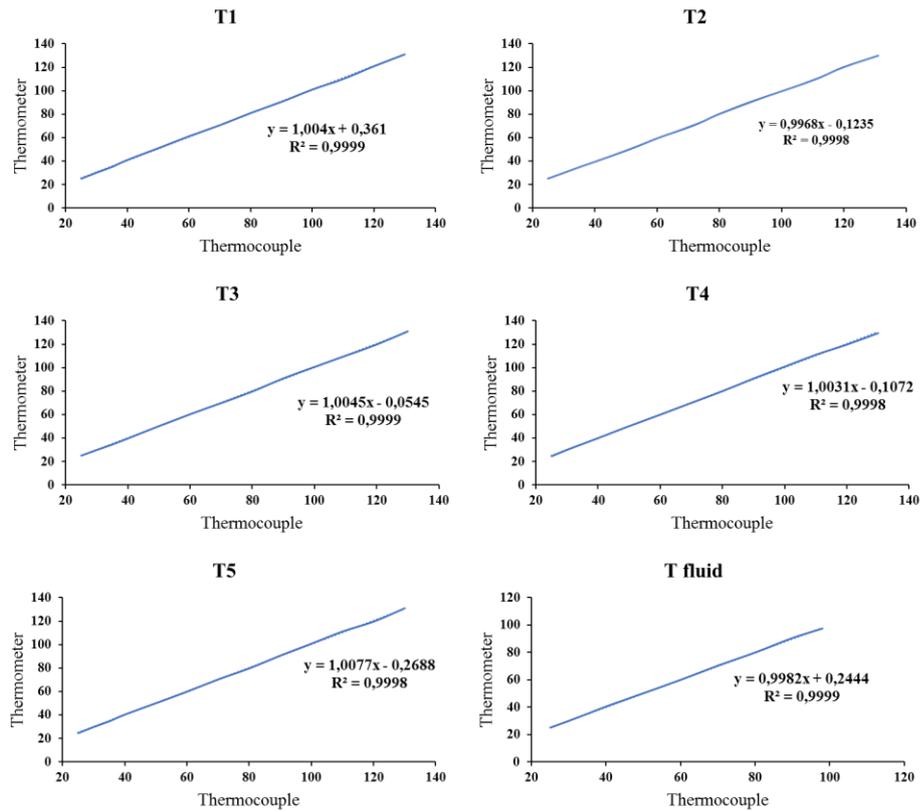
Figure 2–3 Calibration curves for six T-type thermocouples

2-4 Uncertainty Analysis

An uncertainty analysis is used for readings or the related equipment and experimental data related to the experimental parameters based on the error propagation methodology proposed by Coleman and Steele [84]. The general formulation is expressed as:

$$U_y = \sqrt{\sum_{i=1}^{n} \left\{ \left(\frac{\partial y}{\partial x_i} \right) \cdot U_{x_i} \right\}^2} \qquad (3)$$

where U_x is the uncertainty in the parameter X_i. The calculated uncertainties are presented in Table 2-1.

Table 2- 1 Calculated uncertainty for experimental parameters

Parameters	Uncertainty
Volt	±1 V
Amper	±0.1 A
Image pixel size	250 µm
Wall Temperature	±1-5%
Fluid Temperature	±1-4%
Heat Transfer Coefficient	±8-15%
Critical Heat Flux (CHF)	±10-14 %
Bubble departure frequency (Hz)	±4%
Bubble departure volume (mm^3)	±0.05 mm^3

2-5 Data Reduction

The net heat flux is calculated as follows:

$$q'' = \frac{VI - Q_{loss}}{A} \tag{4}$$

Here, V is the applied voltage, I is the current, Q_{loss} is the heat loss and A is the heated surface area. Heat loss is the difference between input power and the amount of cooling energy in single-phase flow regime in boiling experiments. For minimizing the amount of heat loss, the aluminium heating part is surrounded by a Teflon block which is a prevalent as of insulator. To calculate the amount of heat loss for each test, a natural convection analysis was performed. The heat loss is expressed as:

$$Q_{loss} = VI - \dot{m}C_p\Delta T \tag{5}$$

Accordingly, the heat losses are less than 5%. The boiling heat transfer coefficient, h, is calculated as:

$$h = \frac{q''}{T_S - T_f} \tag{6}$$

where T_s is the surface temperature, and T_f is fluid bulk temperature. T_f is measured using a thermocouple, while for saturated boiling the saturation temperature is considered as the saturated temperature at the local liquid pressure. The surface temperatures are obtained by using the thermal contact resistance from the T_{ave} to the silicon surface with the average of the thermocouple measurements, as:

$$T_S = T_{ave} - q'\left(\frac{L_{Al}}{K_{Al}} + R_{TR} + \frac{L_{Si}}{K_{Si}}\right) \tag{7}$$

where $T_{ave} = \frac{T_1 + T_2 + T_3}{3}$ is the average temperature, $R_{TR=}$ 6×10⁻⁶ (m²K/W) is the paste thermal resistance. The difference between saturation temperature, T_{sat} , and the surface temperature, T_s , is defined as the wall superheat ΔT_{sat}.

2-6 Heat Loss Study

To estimate the amount of heat loss, an electrical power is applied to the test section when there is no fluid on top of the heating part. After reaching the steady state condition, the temperature difference between the surface and environment is recorded for each electrical power. Afterwards, recorded electrical power is plotted against the temperature difference of surface and ambient. An equation is obtained by curve fitting which provides the heat loss equation for single and two-phase flow regimes of the experimental setup. To be more exact, the temperature difference between the heating surface and ambient temperature during a real experiment is utilized to estimate the amount of heat loss. The percentage of heat loss is measured between 2.5 to 6 % in the experiments.

2-7 Bubble departure diameter and frequency

Bubble departure frequency and diameter are calculated by averaging the obtained values for at least 10 nucleation sites per case, where 5 sequential bubbles in the images were tracked from growth initiation to the time they reached to the middle of the image frame. Manual pixel-wise calculation is used to determine the locations of diametrical points on bubbles. For each time interval, the bubble centroid location is obtained by averaging the diametrical x and y coordinates. When the bubble radial growth becomes constant, time history of vertical position of the bubble centroid approximates the bubble departure frequency. This approximation is in agreement with Rayleigh [85], Mikic, Rohsenow, and Griffith [86].

Due to constant radial growth rate assumption for attached bubble, the centroid location shows a linear change. Straight lined is fitted to the growth and rising portions. The intersection of the growth line with horizon (x-axis), and growth line and rising lines give the initiation and departure points, respectively. The proposed calculations are in parallel with the method recommended by McHale and Garimella [87].

The general governing equation and boundary conditions for the freely rising bubble is given as follow:

$$\ddot{y} + \frac{3}{4}\frac{\rho_l C_D}{\rho_v D}\dot{y}^2 = \frac{(\rho_l - \rho_v)g}{\rho_v} \tag{8}$$

$$y(t_0) = y_c|t = t_0$$

$$\dot{y}(t_0) = \dot{y}_c|t = t_0$$

The first term in the left side indicates the acceleration of the rising bubble, the second term in the left side are included to inspect the effect of drag force, and the right hand side brings up the importance of buoyancy force effect on rising bubble. Consequently, the drag coefficient of a bubble, time of departure, gravitational acceleration, position and densities of liquid and vapor phases are represented as C_D, t_0, g, y, ρ_l and ρ_v, respectively. The drag coefficient values in the range of 0.14~1.22 are used in the analysis (according to the proposed values in correlations of Michaelides [88] and Ishii and Zuber [89], respectively).

CHAPTER 3: Surface modifications for phase change cooling applications via crenarchaeon *Sulfolobus solfataricus* P2 bio-coatings

3-1 Preface and Objective of Study

Due to its high heat removal capability and exploitation of latent heat, boiling is considered to be one of the most effective cooling methods in industry. Surface structure and wettability are two factors imposing boiling phenomena. Here, we propose an effective and facile method for surface enhancement via crenarchaeon *Sulfolobus Solfataricus* P2 bio-coatings. The positive effects of such surfaces of bio-coatings were assessed, and enhancements in heat transfer and cooling were obtained. Visualization was also performed, and bubble dynamics of generated bubbles and vapor columns from the tested surfaces with bio-coatings are here presented. Superior performance in terms of boiling heat transfer and cooling was reached with the use of crenarchaeon *Sulfolobus Solfataricus* P2 coated surfaces. Thus, this study clearly demonstrates the potential of futuristic surfaces with bio-coatings to achieve substantial energy saving and efficiency.

Here, we propose a novel bio-coating for enhancing heat transfer and CHF in pool boiling via Sulfolobus solfataricus P2, which is a thermophilic archaeon. Nowadays, they are known to be a large and diverse group of organisms which are widely distributed in nature and are common in all habitats[90]. They are divided into five phyla [91, 92]. Archaeon cells have characteristics similar to those of eubacteria, including unicellular morphology. They have a circular chromosome and resemble eukaryotic cells due to their metabolisms involving DNA replication and transcription [93, 94]. Most strikingly, archeal cells have unique habits to keep themselves alive under physiologically harsh conditions such as low or high temperatures (-2 °C to 15 °C or 60 °C to 122 °C), high salinity (2M to 5M NaCl), and low or high pH (<4 or >9) [95-97]. The hyperthermophilic archaeon called Sulfolobus solfataricus belongs to the

Crenarchaeota phylum. It was first isolated by Pisciarelli Solfatara in Italy [98]. Sulfolobus solfataricus is an irregular and lobe-shaped archaeon with a size in the range of 0.2 to 2 µm, which grows optimally at 80 – 85 °C, has a pH of around 3 (while maintaining intracellular pH around 6.5), and can utilize variable carbon sources to maintain cellular homeostasis [99]. The proposed bio-coating is environmentally friendly and is known to be a large and diverse group of organisms. It can endure severe environmental conditions. In addition to abundancy of the Sulfolobus solfataricus P2, the coating process is cheap and fast compared to other bio-coating processes. The coating process was optimized before performing the boiling experiments. It is known that heating temperature and evaporation time are two main factors affecting the cure heat process. Therefore; different configurations were examined to optimize the coating method. Using this coating method, it is possible to soak the interested part of device with an arbitrary geometry into the mixture and obtain the desired coating thickness. In this thesis, we propose a new bio-coating, which is highly durable, environmental friendly, cheap and has a practical coating method and unique structure, which makes the proposed bio-coating a remarkable candidate for heat transfer applications. Thus, this robust and heat resistant microorganism is a good candidate for providing organic porous coatings for energy saving and efficiency in an economical, facile and environmentally friendly fashion, which constitutes the motivation behind this method.

To investigate the effect of thermophilic crenarchaeon bio-coatings on boiling heat transfer and CHF, pool boiling experiments were conducted on silicon surfaces which were coated with different concentrations of thermophilic archaeon. Two solutions of Poly-L-lysine to archaeon with ratios of 1:2.5 and 1:5 were used to coat silicon samples, which led to archaeon layer thicknesses of 1 and 2 µm. All the experiments were conducted with deionized water under atmospheric conditions. The test area (sample size) was as 1.5×1.5 cm^2.

3-2 Sample preparation and charcterization

All the information about crenarchaeon *Sulfolobus solfataricus* P2 preparation and the coating process is shown in Figure 3-1.
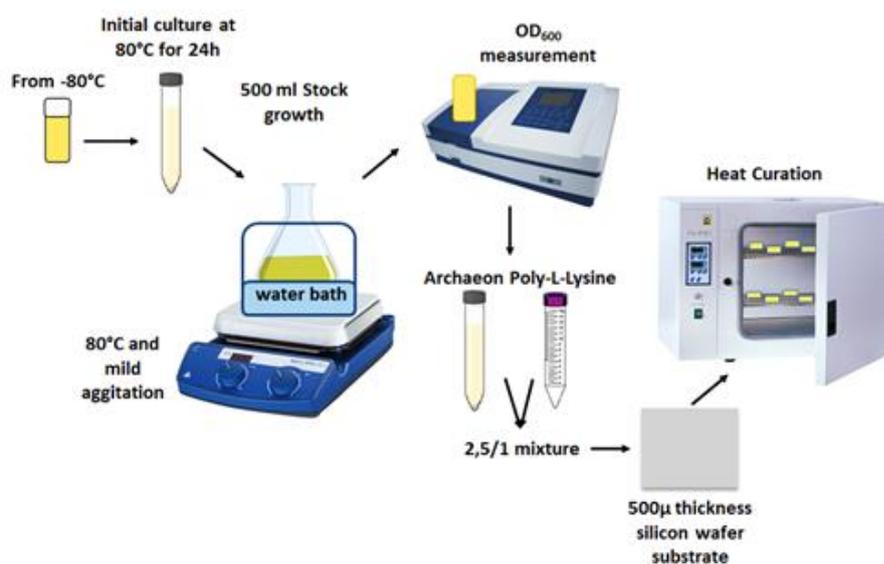
Figure 3–1 Schematic representation of the sample preparation

Sulfolobus Solfataricus is one of the hyperthermophilic and acidophilic archea. It belongs to *Sulfolobus* species and could be a good model for temperature dependent phenomena such as cooling. For this purpose, *Sulfolobus solfataricus* P2, was grown at 80°C, pH of 3 in a batch culture under mild agitation. Basal salt medium, Brock modified Allen medium [100] were used to obtain optimal growth. However, as the salt medium is based on minimal media containing only minerals as a carbon source, we supplemented the basal medium with different concentrations of Sucrose (0.5, 2.5 g/L) with 0.2 % (w/v) Tryptone. Stock cultures were maintained in 2g sucrose/L and 100g glycerol/L. Cultures were started from −80 °C stock; cells were inoculated into 50 mL fresh culture medium. After 24 h of propagation, the cell culture was transferred to 500 mL of the pre-heated new medium. Cell growth was then monitored with UV Spectrophotometer at 600 nm following each 24 h till 96 h. 1ml of cells were pelleted at 4000 g for 5 min and then re-suspended in 500 μl of 4 % (v/v) PFA for 20 min and then permeabilized with 0.1% (v/v) Triton X-100 at RT for 5 min. Fixed and

20

permeabilized cells were washed with PBS buffer twice and then cells were spread on Poly-L-lysine coated cover slide. After air-drying, cells were stained with DAPI (4',6-diamidino-2-phenylindole, 10 µM). Then, coverslides were mounted and inspected under 40X magnification using a BX60 fluorescence microscope (Olympus, BX60, Japan).

The bio-coated surfaces were produced on 500µm thick silicon wafer substrates with the heat cure method, which is easier and less expensive than other coating methods. Surface porosity, roughness and wettability are three main factors directly affecting phase change process on a surface. As a result, the coating process was optimized before performing the boiling experiments. Accordingly, different parameters such as heating temperature, and evaporation time were altered to obtain the optimized surface morphology (as shown below).

Table 3- 1 Optimization of heat cure method

Test #	Temperature (°C)	Duration (min)
#1	35	60
#2	40	50
#3	60	35
#4	80	15
#5	35	50
#6	40	30
#7	60	20
#8	80	10
#9	35	40
#10	40	40
#11	60	40
#12	80	20

According to the obtained results, the test #7 has the optimum surface morphology. It should be noted that the coating method did not change the surface morphology substantially, implying that Sulfolobus solfataricus P2 provides the structured porous surfaces.

Below, SEM images for different surface treatments are displayed.

35°C – 50 min   60°C – 35 min

80°C – 15 min   80°C – 20 min
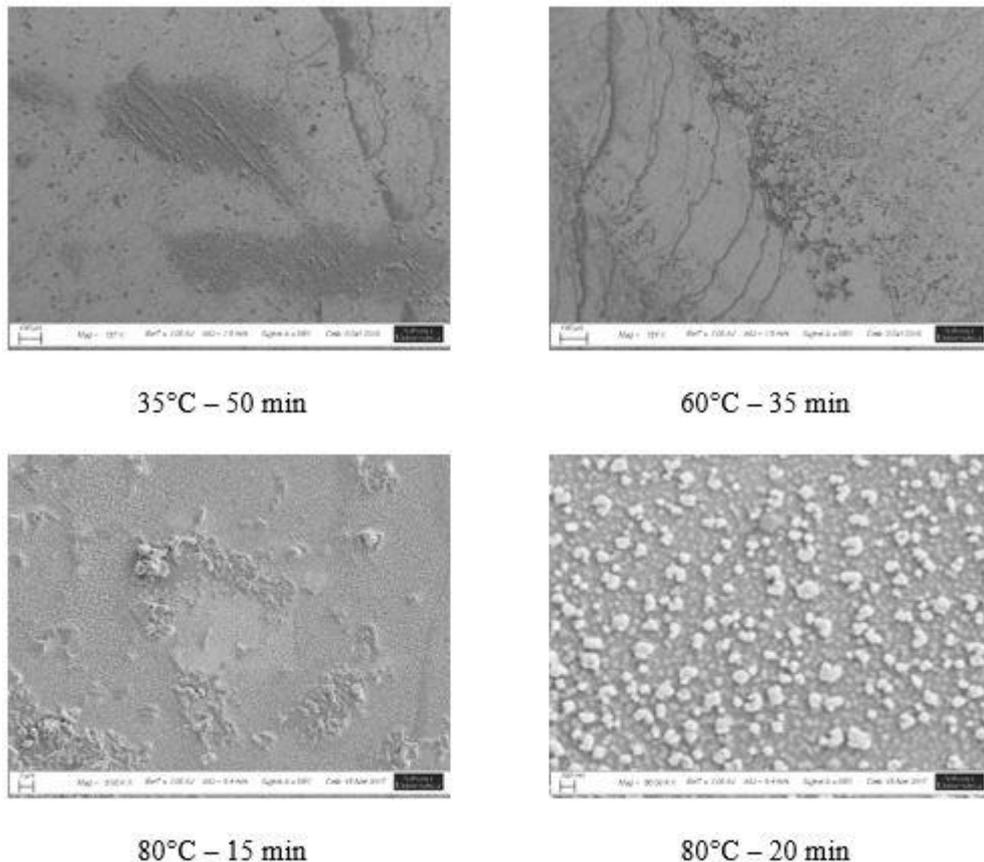
Figure 3–2 SEM images of various heat cure optimization

The cavity size distribution of more than 20 samples coated with optimized method were compared, and according to obtained results, the cavity size distribution was directly affected by the concentration of bio-mixture, the temperature of the oven, the time of evaporation. The reported data is from a sample with the average cavity size among the samples.

In order to ensure the repeatability of the examined surfaces, the samples were characterized before and after each experiment. A scanning electron microscope (FEG-SEM Leo Supra 35, Oberkochen, Germany) was used to obtain the microstructural images of the specimen surfaces before and after the treatment. SEM scans an electron beam on the surface of a specimen and measures a number of signals resulting from the

interaction between the beam and specimen. One particularly useful imaging method is collecting low energy secondary electrons (SE) signals, which originate within a few nanometers from the specimen surface. Due to this process, SE method allows imaging of the surface with a high spatial resolution. The micrographs were collected using SE mode in low voltage (2 KV) within different tilts to allow a full imaging of the surface area and the cross sectional area. The wettability of bio-coated surfaces was tested by the WCA (water contact angle) method. The Sessile drop method was used to measure the CA (contact angle) by dispensing a 5 μL water drop, and the average CA from five different positions on each sample was taken into consideration. The dynamic contact angles were measured by holding the water drop with a stationary needle in contact with the surface and moving the goniometer stage along one direction. The surfaces were tilted at an angle of 25° relative to the horizontal direction. To check whether the angles are the true advancing and receding angles, the surface was further tilted to 50°. The angles remained nearly unchanged implying that these were representatives of the advancing and receding contact angles, respectively.

The coated surface structures were analyzed and characterized using Scanning Electron Microscope (SEM) techniques.
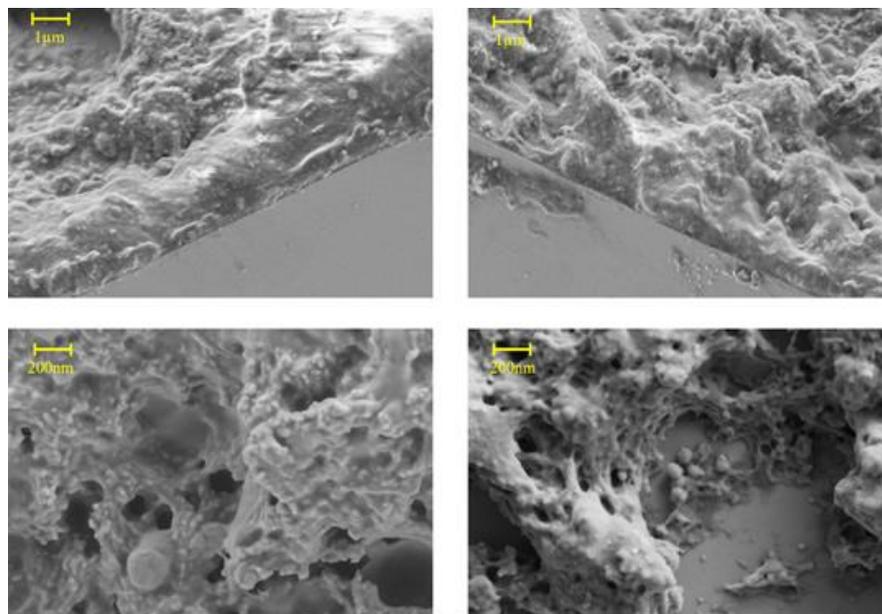
Figure 3–3 SEM images of the optimized morphology

Cavity size, shape, range and distribution along the surfaces were obtained using the 2-D and 3-D surface profilometer technique. Furthermore, surface wettability was measured with the contact angle measurement technique. Fig. a, Fig. b, and Fig. c show

the 2-D surface profile, cavity size distribution, and 3-D surface profile of the coated sample with the thickness of 2µm, respectively. As can be seen, large colonies with structures of a minimum height of 1µm are located separately with distances between them up to 100 µm, which creates a nano-micro interconnected porous medium. This medium can also be observed in the SEM image (Fig. f). The cavity size distribution (Fig. b) indicates that more than 60 percent of the surface is coated with large colonies with sizes bigger than 4µm. The static contact angle measurements of the silicon wafer and bio-coated silicon wafer are presented in Fig. d, which shows that surfaces with bio-coatings have a higher wettability. On the other hand, dynamic contact angle measurements on the bare, 1µm, and 2µm coated surfaces have receding contact angles of ~51°, ~18°, and ~15°, respectively. This highlights the pronounced wetting behavior of the coated surfaces in boiling, especially prior to the critical heat flux condition. The porous nano-micro structures provided by such bio-coatings offer separate channels to intensify wicking flows through the media. The interconnected porous media are responsible for the lower contact angle followed by higher surface wettability, which also generates capillary motion within pores in such structures. This observation agrees with the reported data reported by Singh et al. [101] and Das et al. [102] .
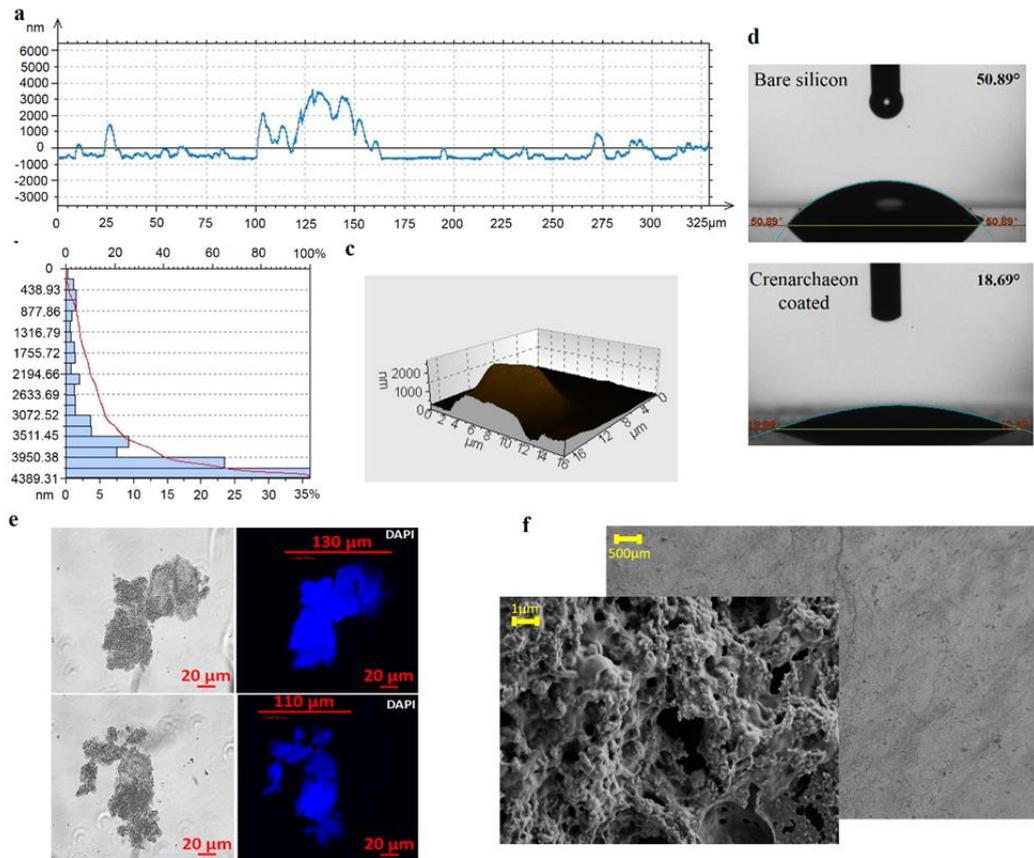
Figure 3–4 Samples were characterized before and after each experiment using the scanning electron microscope, Profilometery and contact angle measurement techniques and Fluorescence micrograph of cellular structure from archaeon (a) 2-D surface profile showing the cavities size and shape on the tested samples (b) Cavity size distribution showing the distribution of the cavities on the tested samples. (c) 3-D surface profile of a cavity with ~2µm (d) water contact angle measurement on silicon surfaces and 1µm crenarchaeon coated samples (e) Fluorescence micrograph of cellular structure from archaeon. DNA stained by DAPI (Blue) (f) SEM images of coated surface showing surface porosity

3-3 Heat Transfer Performance

Before conducting pool boiling experiments on bio-coated surfaces, the independency of the results from the Poly-L-lysine adhesive layer was tested (as stated in the sample preparation section, Poly-L-lysine was used for transferring crenarchaeon coatings on the silicon surfaces). By comparing the obtained results from the bare silicon surface and the Poly-L-lysine coated silicon surface (Figure 3-5a), it seen that the adhesive layer had no effect on pool boiling heat transfer.

Crenarchaeon coatings with two different thicknesses were used to investigate the effect of the proposed bio-coating thicknesses on the pool boiling heat transfer performance. Figure 3-5a shows the obtained heat flux-wall superheat profiles for different examined surfaces. As can be seen, an increasing trend is observed for all the tested samples. The obtained results indicate that for a constant wall heat flux, significant lower wall temperatures were obtained on bio-coated surfaces (for both thicknesses) at the same heat flux compared to the uncoated samples. In other words, the rate of wall superheat increase is much lower for crenarchaeon coated surfaces relative to that of the bare and Poly-L-lysine coated surfaces. Furthermore, it can be observed that wall superheat increase decreases with coating thickness at a fixed wall heat flux.

The heat transfer coefficient profile is shown in Fig. 4b. At a fixed heat flux, heat transfer coefficients obtained from the crenarchaeon coated surfaces are higher than those of the bare silicon surface, while the heat transfer coefficient increases with the coating thickness. Maximum enhancements of 94.2% and 126.7% were obtained for 1μm and 2μm thick coatings, respectively, in comparison to the bare silicon surfaces.

The critical heat flux (CHF) location and corresponding wall superheat are labeled for each sample in Fig. 3a. As can be seen, for all the bare and crenarchaeon coated surfaces, the heat transfer coefficient increases with heat flux until the critical heat flux (CHF) point. According to the obtained results, the CHF of the bare silicon surface is measured as 115 W/cm^2 (corresponding wall superheat of 68°C), while CHF values of bio-coated surfaces reach 190.75 (corresponding wall superheat of 64.8°C) and 229.16 W/cm^2 (corresponding wall superheat of 57.8°C) for surfaces with coating thicknesses of 1μm and 2μm, respectively. It can also be observed that CHF increases with coating thickness.
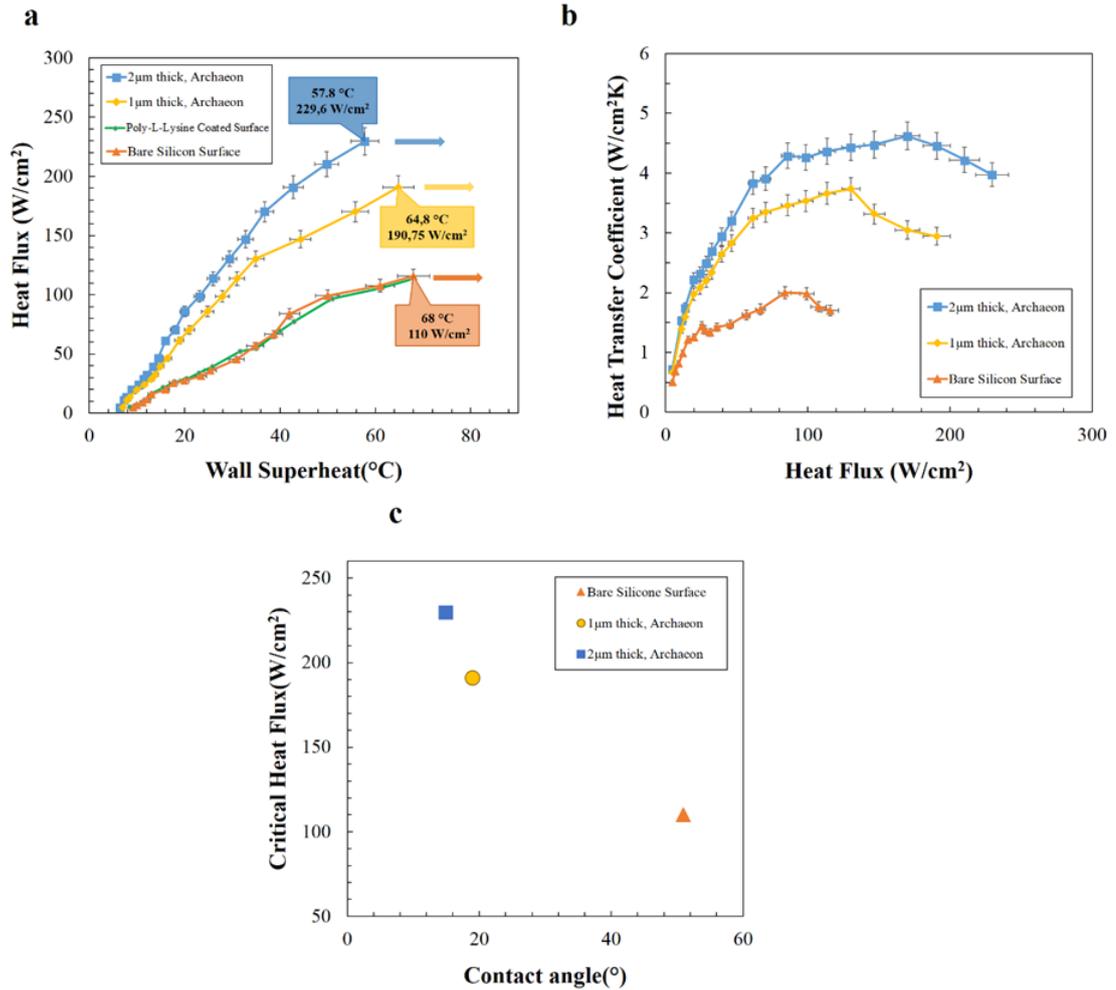
Figure 3–5 . Heat transfer coefficients for coated and plain surfaces. The effect of coating thickness on heat transfer performance of the surfaces was obtained using applied wall heat flux, wall and fluid temperatures. Critical heat fluxes and enhancements via bio-coated surfaces are presented. (a) wall superheat-heat flux profile (b) heat flux-heat transfer coefficients profile (c) obtained critical heat flux values as a function of surface contact angle

3-4 Discussion

Surface modification is one of the most used techniques for heat transfer and critical heat flux enhancement in heat transfer applications involving phase change. Heat transfer results indicated that the crenarchaeon and their aggregates form a bio-coating on the surface, which changes the surface structure for better heat removal. While chemical surface treatments are severely toxic, such bio-coatings are suitable candidates to change the surface structure in an environmental friendly and biocompatible fashion.

27

Interactions between surfaces and organisms were investigated and different biological structures such as complex microbial communities (bio-films) were reported. Studies revealed that archaeal species adhere to either biotic or abiotic surfaces, and they are able to form multicellular complex bio-film structures under a wide range of extreme environmental conditions including hydrothermal vents, under water springs of the Dead sea or on walls of sulfide-rich cave system together with bacteria [103-106]. Cellular aggregation and proliferation mediated by flagella or type IV pili maintain the mature architecture of these structures [100, 107]. Furthermore, they were also embedded in a mesh of proteins, polysaccharides and lipids called EPSs (extracellular polymeric substances), which can further modify the surface [108, 109].

Sulfolobus species can also form different types of architectures on the surface. *Sulfolobus Solfataricus* species form flat bio-films with low cell density, while *Sulfolobus acidocaldarius* species lead *to* bio-films with tower-like aggregates [110]. The archaeal pili of *Sulfolobus Solfataricus* are found to mediate surface adhesion [109]. Moreover, mutant strains showed the importance of the pili function and the structure for the architecture [109, 111, 112]. The studies reported that the amount and composition of the EPSs are involved in the formation of the architecture, and the first enzyme, which affects EPSs, is identified in *Sulfolobus Solfataricus* [113]. In addition, environmental conditions including temperature, pH, salt concentration and exposure to UV can modify the archaeal communication and ultimately affect the surface structure covered with crenarchaeon [112, 114]. Our results support that monoculture of the crenarchaeon can lead to flat structures through mimicking natural conditions.

The significant enhancements in both CHF and boiling heat transfer with crenarchaeon coated surfaces are attributed to the physical structure of coated surfaces.

As shown in Figure 3-6, the coated layer creates a porous structure with numerous pores, which act as nucleation sites during boiling. The size of pores ranges from 100nm to 2µm. Therefore, the aggregation of these pores produces more nucleation sites on the porous coated layer and result in higher heat transfer rate [115]. This can be clearly examined in Figure 3-6 showing more active nucleate sites on the coated surface compared to the bare silicon surface. The existence of a porous layer has a great effect on liquid transportation inside the structure. There are many interconnected porous channels, which aid liquid transportation between the pores beneath the surface

resulting in the CHF delay [115]. Capillary pumping is another mechanism, which has a considerable effect on the surface rewetting by providing liquid flow to dry spots (Figure 3-6).
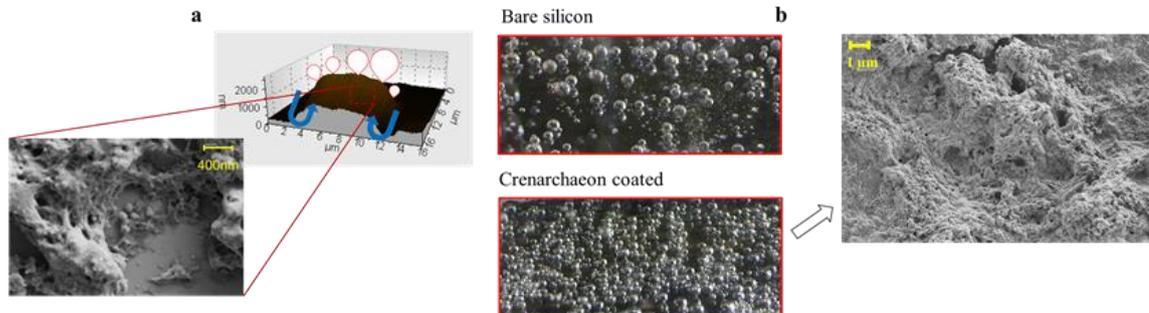
Figure 3–6 Heat transfer mechanism on bio-coated surfaces. a) Wicking flow mechanism b) higher number of active nucleation sites

In other words, capillary flow reduces liquid-vapor counter flow resistance by providing flow path for liquid and vapor and prevents the dry-out condition [116]. In the literature [117] , a method was reported to release trapped vapor in a porous layer by adding vapor channel, which offers paths for escaping vapor. It can thus be hypothesized that the colonial structure of archaeon porous layer can provide separate vapor channels through the porous layer. These channels can release trapped vapor at the bottom of the porous layer, thereby delaying the CHF condition. Electron microscopy and surface profile images (Figure 3-3 and Figure 3-4) indicate that the crenarchaeon coatings are distributed over the surface like separated colonies with a minimum size of 1um. The distance between these colonies are coated with layers of archaeon acting as channels for vapor venting inside the porous layers. These channels not only remove the vapor layer at the bottom of porous structure but also separate the vapor and liquid path flow, which is another reason for CHF and HTC enhancement [117].

The effect of bio-coatings was also examined using images from the high-speed camera (250 frames/sec). Since it was difficult to define the average bubble diameter at high heat fluxes, the bubble departure volume is considered instead of the average bubble departure diameter. Most bubbles are not spherical except at low heat flux ($<60\,\text{W/cm}^2$). Therefore, we assume that all bubbles were ellipsoid, as shown in Fig. 5a. The volume shrinks with the coating thickness. With bio-coatings, bubble release frequency (~7.5 Hz, ~33 Hz, and ~38 Hz for silicon, 1μm archaeon and 2μm archaeon coated surfaces,

respectively, at the heat flux of 56 W/cm^2) increases accompanied with the decrease in the bubble volume, which serves as a proof for the performance and energy efficiency enhancement in phase change systems.
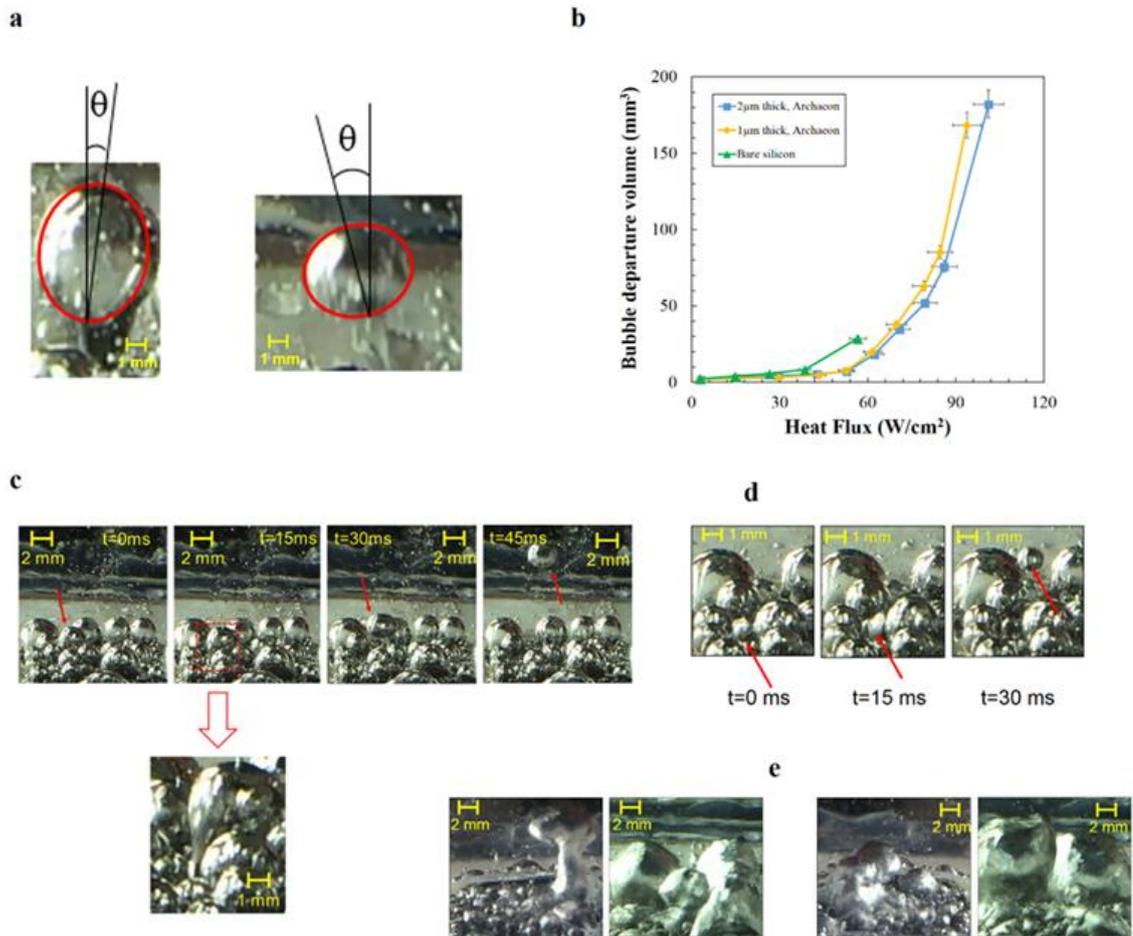
Figure 3–7 Boiling images from coated and uncoated surfaces. Visual results were obtained using the high-speed camera system. Bubble dynamics and vapor columns were investigated in order to have an understanding about the enhancement mechanisms (a) bubble images on coated surfaces at 50 W/cm2. Shape of bubbles is ellipsoid according to the images (b) bubble departure volume of bare silicon (green line), 1µm thick (yellow line) and 2µm thick (blue line) bio-coated surfaces (c) inclined departed bubble (d) isolated bubble in nucleate boiling region (e) vapor columns on uncoated and coated surfaces

CHAPTER 4: Optimum Ratio of Hydrophobic/Hydrophilic Surface Area for Phase Change Cooling Systems

4-1 Preface and Objective of Study

Wettability is one of the most important factors in two-phase heat transfer due to the control of dynamic triple contact lines, which are inter-connected lines for liquid, solid, and gas phases [118, 119]. On the other hand, miniaturization of heat transfer systems leads to the increase in the effect of interfacial forces compared to that of body forces, thereby emphasizing on the important role of wettability in two-phase heat transfer [120]. The role of high surface wettability on CHF enhancement was reported by Wang and Dhir [31]. Two years later, Vinogradova et al [121] reported the fact that nucleation is more likely on hydrophobic surfaces due to higher concentration of trapped air in sub-micron cavities compared to hydrophilic surfaces. While hydrophilicity enhances the CHF limit, hydrophobic surfaces boost the bubble nucleation regime; thereby making the exact effect of wettability on boiling complex. In 2010, Betz et al [122] showed that mixed hydrophilic and hydrophobic surfaces enhance both heat transfer coefficient and CHF. They conducted experiments on hydrophilic networks (hydrophilic surface with hydrophobic islands) and hydrophobic network (hydrophobic surface with hydrophilic islands). They reported that hydrophilic networks with 65% and 100% enhancement in CHF and heat transfer coefficient, respectively, had a better performance by preventing formation of an insulating vapor blanket compared with hydrophobic networks. Afterwards, superbiphilic surfaces had been used to assess the effect of super hydrophilic surface with super hydrophobic islands [123]. In the related study, critical heat fluxes over 100 W/cm^2 and heat transfer coefficients more than 100 kW/m^{2}K were reported.

Although the above-mentioned studies provided valuable data on the combination of hydrophobic and hydrophilic surfaces, the optimum ratio of hydrophobic to hydrophilic surface area has not been taken into account.

This study aims to present a novel fabrication method for biphilic surfaces, to determine the optimum ratio of hydrophobic to hydrophilic area for the highest boiling heat transfer performance, and to assess bubble dynamics on biphilic surfaces. To fabricate biphilic surfaces, deep reactive ion etching (DRIE) and silicon oxide thin films have

been used for hydrophobic and hydrophilic areas, respectively. One hundred hydrophobic islands (10×10) are surrounded by silicon oxide on 1.3×1.3 cm^2 silicon sample. Hydrophobic islands are enlarged step by step to wholly hydrophobic surface. Boiling curves are obtained for all the biphilic surfaces. To analyze bubble dynamics, a high-speed camera was used to record the bubble nucleation and bubble motion during pool boiling heat transfer.

4-2 Biphilic enhanced surface fabrication process

Ten types of mixed wettability surfaces are fabricated. On each sample, one hundred (10×10) hydrophobic circular spots are surrounded by silicon dioxide to achieve biphilic behavior. A central distance of 1mm between hydrophobic islands is kept for all the samples. To find the optimum ratio of hydrophobic to hydrophilic area, the diameter of hydrophobic islands is increased step by step to create a completely hydrophobic surface. All the data related to sample geometries are tabulated in Table 4-1.

Table 4- 1 Geometric properties of the biphilic surfaces

Surface No.	Hydrophobic Diameter (µm)	Edge to edge spacing between hydrophobic spots	Hydrophobic/Total area (A*) %
#1	50	950	0.19
#2	150	850	1.76
#3	300	700	7.06
#4	400	600	12.56
#5	500	500	19.62
#6	700	300	38.46
#7	800	200	50.24
#8	900	100	63.58
#9	1000	-	78.5
#10	1100	-	95
SiO$_2$ Coated Sample		Totally Hydrophilic	
Nano-grass Sample		Totally Hydrophobic	

All the samples are fabricated on 100mm silicon wafers. A schematic of microfabrication process can be seen in Figure 4-1.
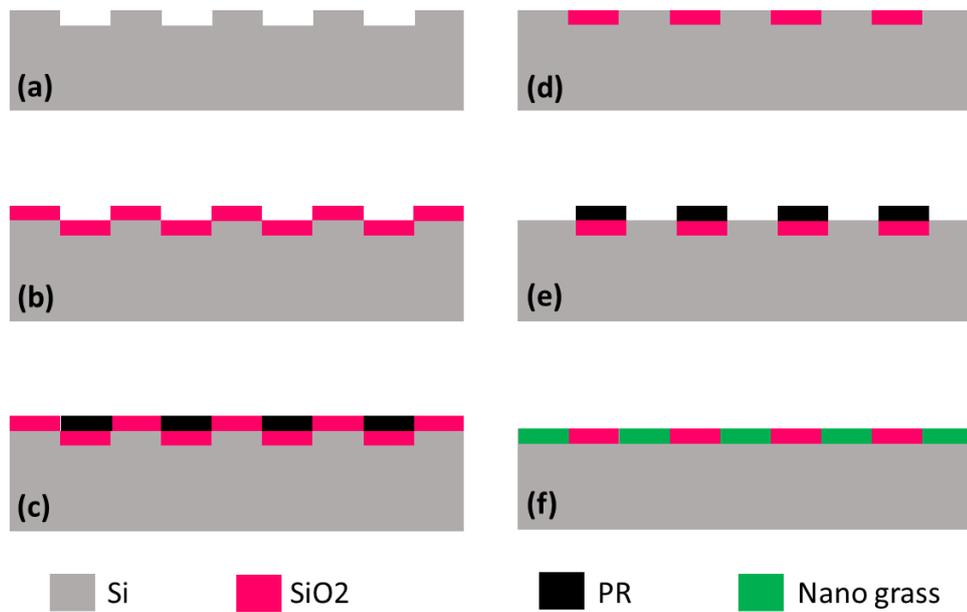
Figure 4–1 Fabrication of biphilic surfaces. a) 1 µm deep anisotropic silicon etch using photoresist as etch mask. b) Thermal growth of 1 µm oxide. c) Photolithography – oxide etching mask. d) Dry etching of silicon oxide. e) Photolithography – silicon etching mask. f) Formation of nano grass using deep silicon etching

Firstly, to prevent any height difference between hydrophilic and hydrophobic areas, substrate of hydrophilic network is etched for 1µm. A patterned 2µm thick photoresist (AZ-ECI) is used as an etch mask to protect the areas, which will become hydrophobic islands. A 1µm-thick layer of SiO_2 (hydrophilic material) is grown on the Si substrate using wet thermal oxidation (Figure 4-1b). Afterwards, a patterned 2µm thick layer of photoresist is used to protect SiO_2 hydrophilic network during the silicon dioxide dry etching (Figure 4-1c).

After etching SiO_2 and removing photoresist (Figure 4-1d), the third patterned layer of photoresist is used as an etch mask to protect hydrophilic areas during the fabrication of hydrophobic spots via deep reactive ion etching (Figure 4-1e). In the last step, the black silicon method [124] is used to fabricate nano-grass on the silicon substrate. Although there are several studies on the fabrication of needle-shaped structure in the literature [125, 126], the given information and recipe for a specific process cannot be used directly in other laboratories. This issue results from the difference of etcher configuration, chamber geometry, and flow handling of various etching equipment [124]. The formation of nano-grass structures is sharply dependent on etching

parameters such as gas flows and chuck temperature [127]. Here, the idea is to use SF_6 and C_4H_8 gas flows with manipulating pulse time of SF_6 to control passivation layer. The pulse time of SF_6 varies from 3 to 4 with various chuck temperatures ranging from 30˚C to 0˚C. The process parameters of the 5 tested different recipes can be seen in Table 4-2.

Table 4- 2 Nano-grass etching parameters. 5 different etch recipes were tested. The gas flows of SF6 and C4H8 are fixed at 300 sccm and 150 sccm, respectively. The SF6 pulse time is either 3 or 4 seconds and the C4H8 pulse time is fixed at 2 seconds. The chuck temperature is varied between 0˚C and 30˚C. The etch time is 3 min in all cases

Recipe name	SF_6 (sccm)	Pulse time (s)	C_4H_8 (sccm)	Pulse time (s)	Chuck temperature (˚C)	Etch time (min)
N-G #1	300	3	150	2	30	3
N-G #2	300	4	150	2	30	3
N-G #3	300	3	150	2	10	3
N-G #4	300	4	150	2	10	3
N-G #5	300	3	150	2	0	3

After etching process, to check for the quality of samples, all of them are checked by eye. Recipes N-G #1 and N-G #4 are eliminated due to the low quality of etching. Figure 4-2 shows scanning electron microscope pictures of the fabricated samples using N-G#2, N-G#3 and N-G#5. The formation of nano grass is poor when N-G#2 recipe has been used.
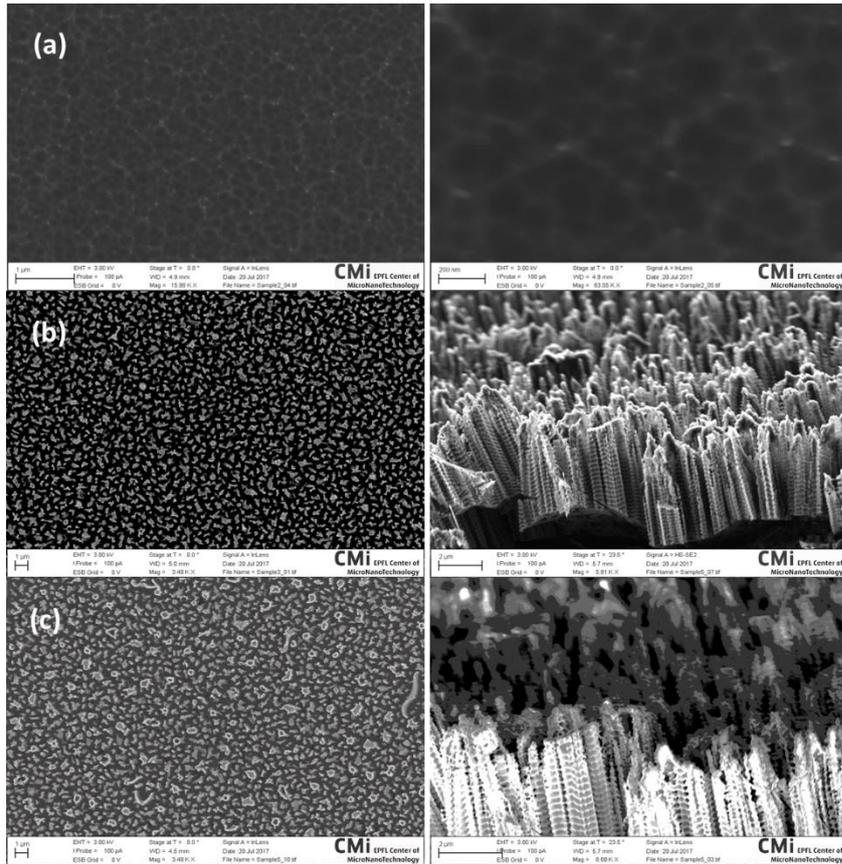
Figure 4–2 SEM images related to recipe (a) N-G #2 (b) N-G #3 (c) N-G #5

The SEM images of fabricated samples are shown in Figure 4-3. As can be seen, hydrophobic islands become gradually bigger step by step, so that an optimum morphology could be obtained for phase-change heat transfer.
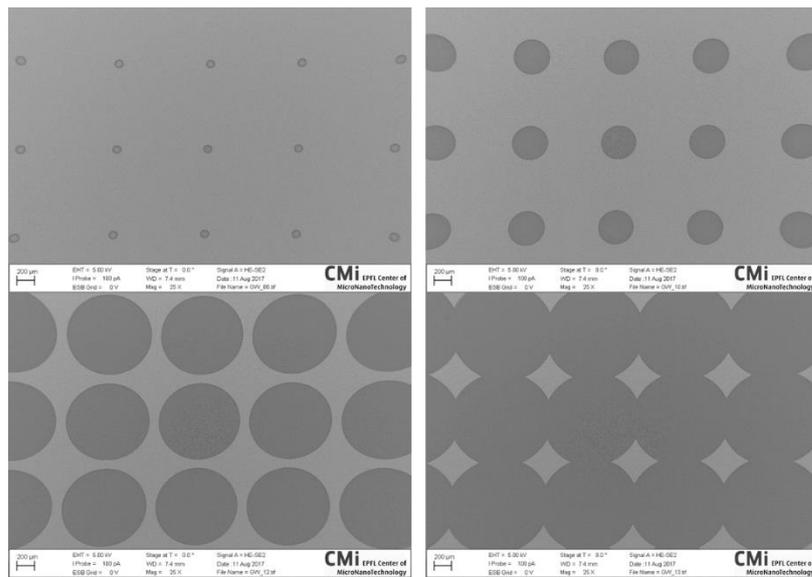
Figure 4–3 SEM images related to fabricated samples

4-3 Surface Characterization

The surface morphology of nano-grass and mixed hydrophilic and hydrophobic samples is obtained via Scanning Electron Microscopy (SEM, Z15-Zeiss-Merlin).

With the use of scanning probe microscopy (SPM) methods, the topographical imaging of surfaces is extensively available. The characterization of surface structures such as topographical shape and characteristics can be analyzed with the SPM method. The enhanced surfaces are characterized by Atomic Force Microscopy in dynamic mode (ezAFM, Nanomagnetics Instruments). 2-D and 3-D AFM results are presented in Figure 4-4 (a) and (b). As can be seen, the average height of microstructures is equal to 1µm, which suggests that there is no height difference between hydrophilic and hydrophobic parts.

The wettability of enhanced surfaces is tested by the WCA (water contact angle) method by ThetaLite Tensiometer (Dyne Technology). The Sessile drop method is used to measure the CA (contact angle) by dispensing a 5µL water drop. Contact angles of 20° and 165° are measured for hydrophilic and hydrophobic parts, respectively.
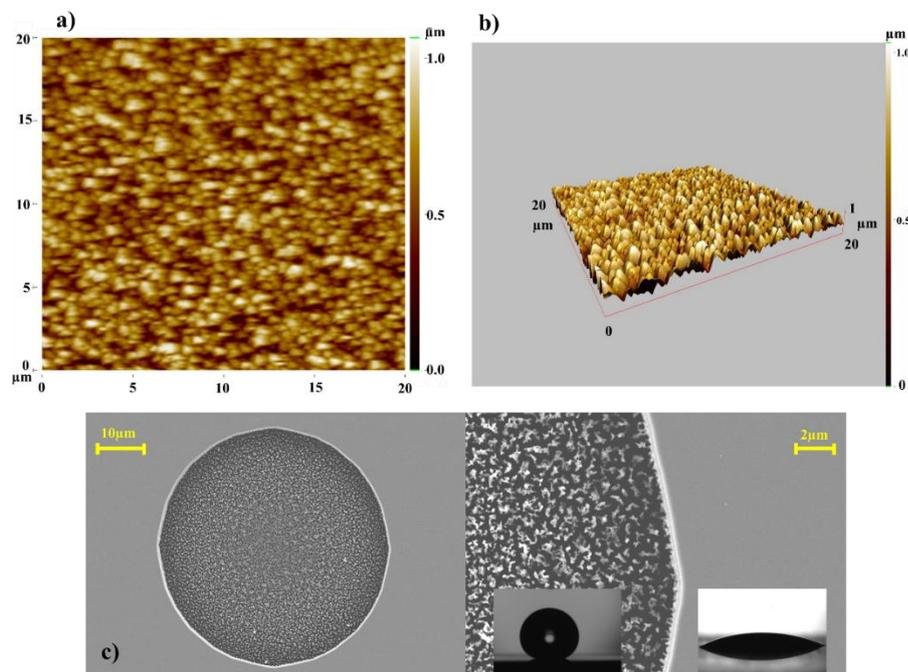
Figure 4–4 Surface characterization of biphilic samples. Samples are characterized using atomic force microscopy (AFM) and contact angle measurement. a) 2-D b) 3-D AFM results showing the size and shape of hydrophobic structures. c) Contact angle measurement on both hydrophilic (20°) and hydrophobic (165°) areas.

4-4 Results

Surface wettability plays a crucial role on boiling heat transfer. On one hand, hydrophilicity effectively suppresses bubble nucleation and departure process, leading to delayed CHF. On the other hand, hydrophobicity promotes bubble nucleation, resulting in higher HTC values. A smart combination of these characteristics leads to an enhancement results in much improved boiling efficiency. For this, we examined biphilic surfaces (surfaces with mixed hydrophilic/hydrophobic patterns) with various ratios of hydrophobic to hydrophilic areas to find the optimum ratio of mixing wettability for enhancing boiling heat transfer coefficient (HTC) and critical heat flux (CHF). It should be noted that before examining biphilic surfaces, pool boiling experiments were performed on hydrophilic and hydrophobic surfaces. Accordingly, CHF values of 98 W/cm^2 (corresponding wall superheat of 49 K) and 56 W/cm^2 (corresponding wall superheat of ~40 K) were obtained for hydrophilic and hydrophobic surfaces, respectively.

The boiling curves of the tested samples are shown in Figure 4-5. The endpoint of boiling curves represents the critical heat flux conditions, identified by an immense and sudden increase in wall temperature. In addition to wall temperatures, using a high-speed camera CHF conditions were ascertained by observing vapor blanket formation on the samples. The obtained results revealed that the biphilic samples depending on the hydrophilic to hydrophobic area ratios showed different CHF enhancement and deterioration performances. As an example, for samples #1 (A*=0.19) to #6 (A*=38.46), CHF values increases with the extent of hydrophobic areas on the surface. Accordingly, the obtained CHFs (and corresponding enhancement with respect to hydrophilic surface) for #1, #2, #3, #4, #5, and #6 surfaces are 170 W/cm^2 (73.5%), 176 W/cm^2 (79.6%), 183 W/cm^2 (87%), 191 W/cm^2 (95%), 194 W/cm^2 (98%), and 197 W/cm^2 (103%), respectively.

On the other hand, from sample #6 to #10 a dramatic reduction in CHF values was observed. Although depending on the applied heat flux enhanced surfaces of #7, #8, #9 and #10, provide higher efficiency respect to fully hydrophilic surface, the CHFs (and corresponding enhancement with respect to hydrophilic surface) are depreciated to 142

W/cm^2 (45%), 127 W/cm^2 (30%), 107 W/cm^2 (10%), and 66 W/cm^2 (-32%) for #7, #8, #9, and #10 samples, respectively.
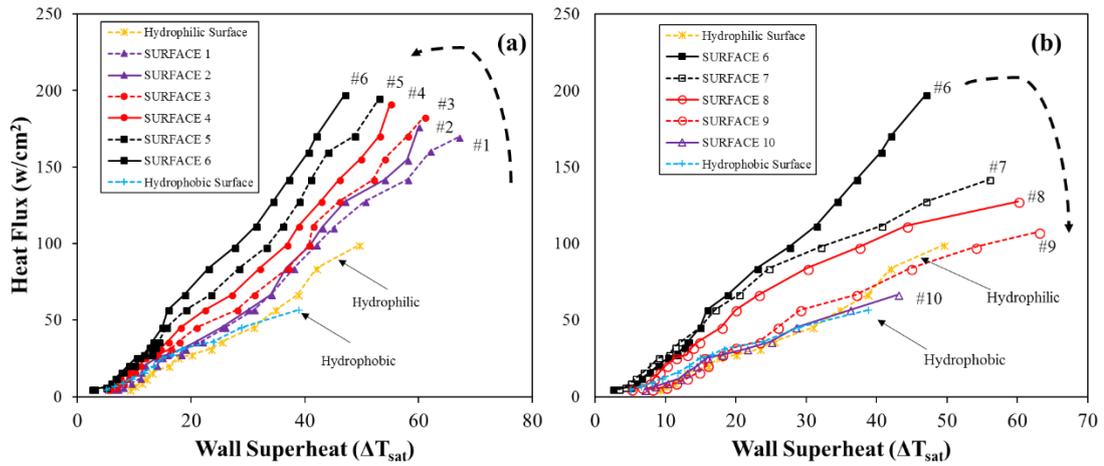
Figure 4–5 The boiling curve for hydrophilic, hydrophobic and biphilic enhanced surfaces. a) Surface #1 to #6. b) Surface #6 to #10.

Heat transfer coefficient (HTC) is the other parameter indicating boiling heat transfer performance of the proposed surfaces. Obtained HTCs are shown in Figure 4-6. Accordingly, all surfaces enhance heat transfer coefficient comparing to hydrophilic and hydrophobic surfaces. While heat transfer coefficient trends of the surfaces #1 (A*=0.19) through #6 (A*=38.46) are increasing for almost all wall heat fluxes, a decreasing trend can be observed for surfaces #7 (A*=50.24) to #10 (A*=95). Heat transfer coefficient trend for the later surfaces can be divided into two groups of low/moderate heat flux (q<50 W/cm^2) and high heat fluxes (q>50 W/cm^2). At low/moderate heat fluxes heat transfer coefficients increase with wall heat flux, where for heat fluxes higher than 50W/cm^2 deterioration in thermal performance of these surfaces were observed. The dominant heat transfer mechanism is nucleate boiling for heat fluxes up to 50W/cm^2. Apart from the ratio of hydrophobic to total surface area, the presence of hydrophobic areas enhances the heat transfer coefficient. This is the main reason for enhanced heat transfer coefficient at low/moderate wall heat fluxes for all of the biphilic surfaces. Due to the early onset nucleate boiling and higher number of active nucleation sites, hydrophobic surface has higher efficiency at low heat fluxes than that of hydrophilic surface. Contrary, at high fluxes, due to the high rate of bubble coalescence and promoted formation of vapor film, a decline in heat transfer coefficient is obvious compare to hydrophilic surface. These results lend support to previous findings in the literature [128, 129].
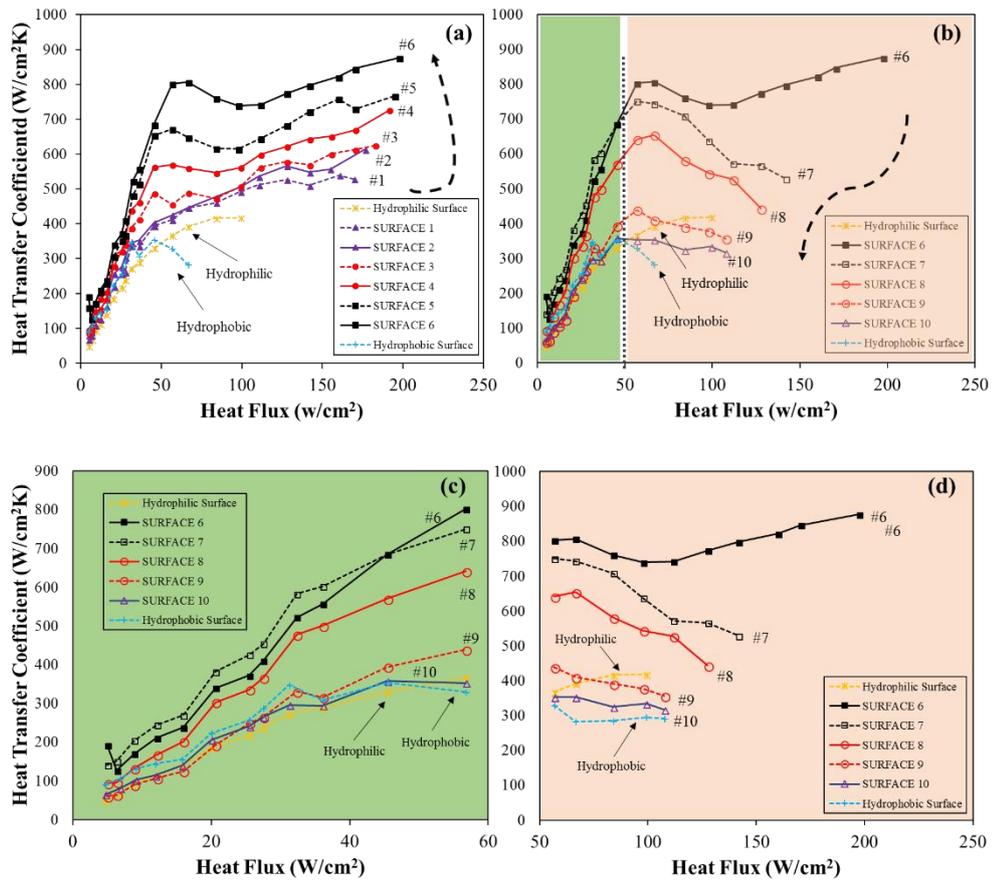
Figure 4–6 Heat transfer coefficient versus heat flux diagram for hydrophilic, hydrophobic and biphilic surfaces a) surface #1 to #6, b) Surface #6 to #10, c) Zoom in data for low heat fluxes of Surface #6 to #10, d) Zoom in data for high heat fluxes of Surface #6 to #10

4-5 Discussion

The nucleation process starts at a lower wall temperature on biphilic surfaces compared to hydrophilic surface, leading to a better boiling heat transfer at low and moderate heat fluxes. As shown in Figure 4-7, bubble nucleation starts from the hydrophobic areas. The small pinning forces of vapor bubbles on hydrophobic areas can substantially enhance the bubble nucleation and departure processes. Due to higher concentration of trapped gas in cavities on hydrophobic surfaces, nucleation is more likely to initiate on hydrophobic surfaces compared to hydrophilic surfaces. Moreover, it is observed that bubble nucleation occurs on the contact line separating hydrophilic and hydrophobic areas. One reason could be due to the wettability induced surface tension gradient. This observation agrees with previous results of Vinogradova et al [121].
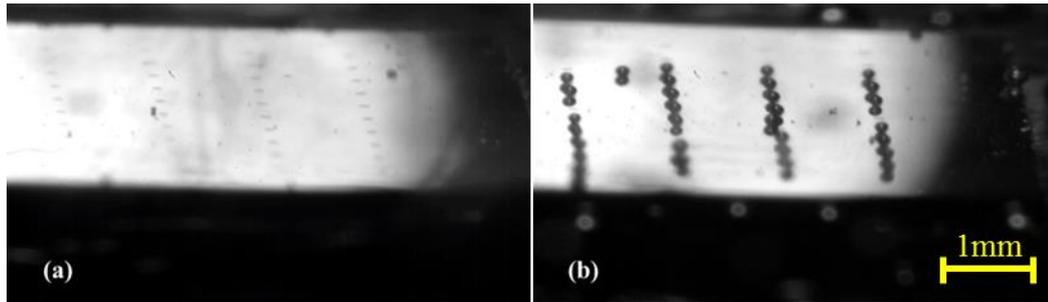
Figure 4–7 The beginning of bubble nucleation on biphilic enhanced surfaces. a) Just before bubble nucleation, b) Right after bubble nucleation

The hydrophobic islands contribute to the increase in bubble departure frequency as well. During bubble departure, while the whole bubble departs from a hydrophilic surface, a small amount of vapor will be left on hydrophobic surface [128, 129], leading to continuous nucleation cycle with no waiting time and higher nucleation frequency relative to the hydrophilic surface. Mikic and Rohsenow have presented a theory on the relation between the nucleate heat transfer coefficient and nucleation site density [130]. They showed that higher number of active nucleation sites lead to higher heat transfer coefficient, thereby supporting our experimental results.

The major parameters for the difference in the amount of heat transfer enhancement among biphilic surfaces are the hydrophilic surface area ratio and diameter, which directly affect bubble nucleation and departure processes and cycle. According to the visualization results, it can be observed that the size of emerging bubbles strongly depends on the diameter of islands, and the size of departed bubbles is dictated by isle spacings. Due to a higher number of active nucleation sites, more bubbles are generated on larger hydrophobic areas and more effective heat transfer can be achieved. The spacing between these islands influences the bubble coalescence and departure process. As can be seen in Figure 4-8, coalesced bubbles on larger hydrophobic islands are widespread on the heated surfaces, while lower number of unified bubbles are observed on surfaces with smaller hydrophobic areas.
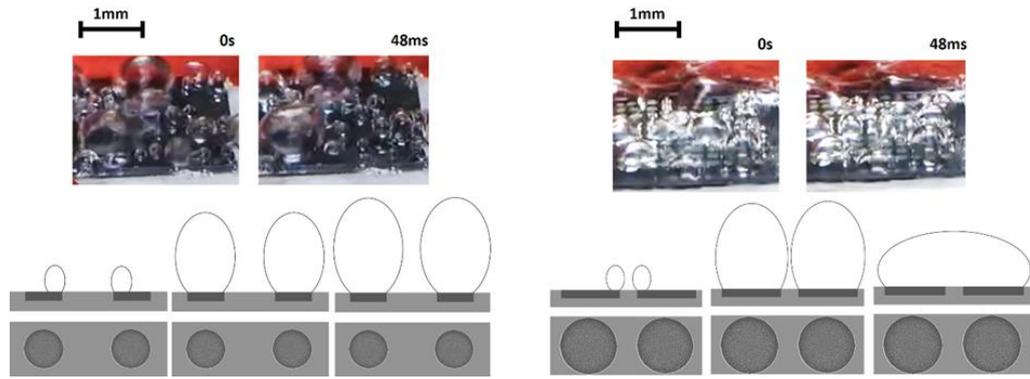
Figure 4–8 The bubble dynamics on biphilic enhanced surfaces along with its schematic at heat flux of 50 W/cm^2, Surface #1 (left side) and Surface #8 (right side)

Hydrophobic island area and edge to edge distance between hydrophobic islands alter the heat mechanism, resulting in an optimum configuration for the maximum heat transfer coefficient at low/moderate heat fluxes. According to the obtained results, surface #6 has the optimum hydrophobic/total area ratio for the maximum nucleate boiling heat transfer. The visualization results reveal that the bubble merging and coalescence take place sooner as hydrophobic island size increases (consequently edge to edge distance decreases), resulting in vapor coverage on the surface, which implies earlier bubble coalescence and a higher chance for vapor blanket coverage on the surface with larger hydrophobic areas and shorter edge to edge distance. Also, the vapor coverage on the biphilic surfaces suppresses microlayer evaporation (the dominant heat transfer mechanism at higher heat fluxes), resulting in heat transfer deterioration on surfaces with higher hydrophobic/total area ratio. Figure 4-9 shows the bubble coalescence and departure on the surface #6. As seen, most of the bubbles depart from the surface before creation of vapor blanket (comparing to Figure 4-8) on the enhanced surface, which is result of the optimum edge to edge distance between hydrophobic islands.

Figure 4–9 The bubble dynamics on the biphilic surface, Surface #6 at heat flux of 85 W/cm^2

At high heat fluxes, isolated hydrophobic areas constrain the bubble nucleation sites, resulting in late CHF occurrence. Moreover, according to the bubble dynamics, the boundary line between hydrophobic and hydrophilic areas prevents spreading of the vapor along the heating surface. Since CHF occurrence is a result of vapor spreading on heater surface, enhanced biphilic surfaces contribute to CHF enhancement by controlling the vapor propagation on the enhanced biphilic surface. This result is in agreement with reported data by Gong and Cheng [131]. Furthermore, hydrophilic parts contribute to the delay in CHF condition at high heat fluxes by promoting microlayer evaporation mechanism underneath the bubbles and rewetting ability [23, 129]. The combination of these features plays the major role in enhancement of both boiling heat transfer coefficient and CHF on biphilic surfaces.
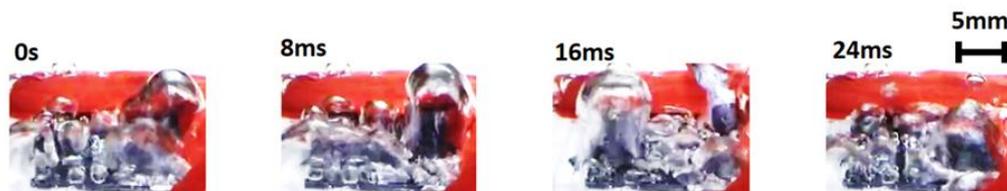
Figure 4–10 Vapor column behavior just before CHF condition (176 W/cm^2) on biphilic surface #6

CHF and heat transfer coefficient enhancement relative to the wholly hydrophilic surface are presented in Figure 4-11. As can be seen, the average maximum enhancements correspond to surface #6. Enhanced biphilic surfaces offer a higher heat transfer performance compared to the wholly hydrophilic surface.
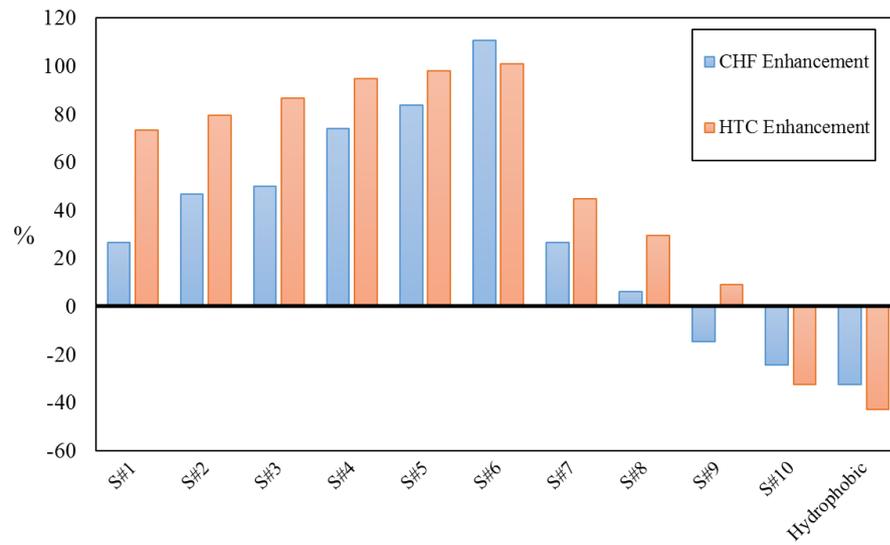
Figure 4–11 The average maximum CHF and heat transfer coefficient enhancements relative to the wholly hydrophilic surface for enhanced biphilic samples

CHAPTER 5:   CONCLUSION

In this thesis, two different types of enhanced surfaces are proposed high-heat flux cooling applications. Crenarchaeon *Sulfolobus Solfataricus* P2 bio-coatings and biphilic enhanced surfaces are investigated. Major conclusions are listed below seperately:

- We propose crenarchaeon *Sulfolobus Solfataricus* P2 bio-coatings for boiling heat transfer enhancement. The novelty of this study lies in the new type of bio-coating and heat transfer enhancements in nucleate boiling due to its surface morphology. These bio-coatings offer enhanced performance and have the potential for addressing high heat removal requirements in many applications including heating and cooling devices, thermofluidic systems, batteries and microfluidic and nanofluidic devices.

- A novel and facile process flow for fabrication of hydrophobic surfaces is proposed. By performing a parametric study, the optimum ratio for mixed wettability is obtained for maximizing heat transfer enhancement and CHF. Ten biphilic surfaces with $A^*=A_{Hydrophobic}/A_{Total}$ ranging from 0.19% to 95% are tested to assess the effect of heterogeneous wettability on cooling system. Using visualization studies, the enhancement mechanisms via biphilic surfaces are revealed. According to the experimental results, heat transfer coefficient and CHF increase with hydrophobic area up to surface with $A^*=38.46\%$, which resulted in the maximum enhancement of both heat transfer and CHF. Surfaces with $A^*>0.38.46\%$ exhibit a decreasing trend in CHF and heat transfer coefficient enhancement. It was found that the decreasing trend is caused by earlier interaction of nucleated bubbles, thereby triggering the generation of vapor blanket at the lower wall superheat temperatures.

In summary, this thesis proposes biphilic and bio enhanced surfaces for high heat flux cooling applications by widening safe zone condition of high-capacity thermal systems. Both enhanced surfaces showed a considerable heat transfer coefficient and CHF enhancement. Moreover, the durability of such coatings ensures their reliability at high flux conditions. Low-cost and facile fabrication is one of the advantages of biphilic and bio enhanced surfaces, which is interesting for industrial applications.

REFERENCES:

1. Bergman, T.L., F.P. Incropera, D.P. DeWitt and A.S. Lavine, *Fundamentals of Heat and Mass Transfer*. 2011: John Wiley & Sons.

2. Kutateladze, S.S., *Heat transfer in condensation and boiling*. AEC-tr-3770, 1952.

3. Zuber, N., *Hydrodynamic aspects of boiling heat transfer (thesis)*. 1959, Ramo-Wooldridge Corp., Los Angeles, CA (United States); Univ. of California, Los Angeles, CA (United States).

4. Incropera, F.P., *Liquid cooling of electronic devices by single-phase convection*. Vol. 3. 1999: Wiley-Interscience.

5. Kim, J., *Spray cooling heat transfer: the state of the art*. International Journal of Heat and Fluid Flow, 2007. **28**(4): p. 753-767.

6. Zhou, D., C.-Y. Zhao and Y. Tian, *Review on thermal energy storage with phase change materials (PCMs) in building applications*. Applied Energy, 2012. **92**: p. 593-605.

7. Kandasamy, R., X.-Q. Wang and A.S. Mujumdar, *Transient cooling of electronics using phase change material (PCM)-based heat sinks*. Applied Thermal Engineering, 2008. **28**(8): p. 1047-1057.

8. Sadaghiani, A.K., N.S. Saadi, S.S. Parapari, T. Karabacak, M. Keskinoz and A. Koşar, *Boiling heat transfer performance enhancement using micro and nano structured surfaces for high heat flux electronics cooling systems*. Applied Thermal Engineering, 2017. **127**: p. 484-498.

9. Collier, J.G. and J.R. Thome, *Convective boiling and condensation*. 1994: Clarendon Press.

10. Nikolayev, V., D. Chatain, Y. Garrabos and D. Beysens, *Experimental evidence of the vapor recoil mechanism in the boiling crisis*. Physical Review Letters, 2006. **97**(18): p. 184503.

11. Şişman, Y., A.K. Sadaghiani, K.R. Khedir, M. Brozak, T. Karabacak and A. Koşar, *Subcooled Flow Boiling Over Microstructured Plates In Rectangular Minichannels*. Nanoscale and Microscale Thermophysical Engineering, 2016. **20**(3-4): p. 173-190.

12. Thome, J.R., *Boiling in microchannels: a review of experiment and theory*. International Journal of Heat and Fluid Flow, 2004. **25**(2): p. 128-139.

13.   Hendricks, T.J., S. Krishnan, C. Choi, C.-h. Chang and B. Paul, *Enhancement of pool-boiling heat transfer using nanostructured surfaces on aluminum and copper.* International Journal of Heat and Mass Transfer, 2010. **53**(15): p. 3357-3365.

14.   Li, C., Z. Wang, P.I. Wang, Y. Peles, N. Koratkar and G. Peterson, *Nanostructured copper interfaces for enhanced boiling.* Small, 2008. **4**(8): p. 1084-1088.

15.   Chu, K.-H., R. Enright and E.N. Wang, *Structured surfaces for enhanced pool boiling heat transfer.* Applied Physics Letters, 2012. **100**(24): p. 241603.

16.   Ahn, H.S., V. Sathyamurthi and D. Banerjee, *Pool Boiling Experiments on a Nano-Structured Surface.* IEEE Transactions on Components and Packaging Technologies, 2009. **32**(1): p. 156-165.

17.   Kubo, H., H. Takamatsu and H. Honda, *Effects of size and number density of micro-reentrant cavities on boiling heat transfer from a silicon chip immersed in degassed and gas-dissolved FC-72.* Journal of Enhanced Heat Transfer, 1999. **6**(2-4).

18.   Honda, H., H. Takamatsu and J. Wei, *Enhanced boiling heat transfer from silicon chips with micro-pin fins immersed in FC-72.* Journal of Enhanced Heat Transfer, 2003. **10**(2).

19.   Shojaeian, M. and A. Koşar, *Pool boiling and flow boiling on micro-and nanostructured surfaces.* Experimental Thermal and Fluid Science, 2015. **63**: p. 45-73.

20.   Lu, Y.-W. and S.G. Kandlikar, *Nanoscale Surface Modification Techniques for Pool Boiling Enhancement—A Critical Review and Future Directions.* Heat Transfer Engineering, 2011. **32**(10): p. 827-842.

21.   Şeşen, M., C.B. Akkartal, W. Khudhayer, T. Karabacak and A. Koşar. *A compact nanostructure integrated pool boiler for microscale cooling applications.* in *ASME 2009 International Mechanical Engineering Congress and Exposition.* 2009. American Society of Mechanical Engineers.

22.   Bourdon, B., E. Bertrand, P. Di Marco, M. Marengo, R. Rioboo and J. De Coninck, *Wettability influence on the onset temperature of pool boiling: Experimental evidence onto ultra-smooth surfaces.* Advances in Colloid and Interface Science, 2015. **221**: p. 34-40.

23.   Gong, S. and P. Cheng, *Lattice Boltzmann simulations for surface wettability effects in saturated pool boiling heat transfer.* International Journal of Heat and Mass Transfer, 2015. **85**: p. 635-646.

24.   Yang, L.-X., Y.-M. Chao, L. Jia and C.-B. Li, *Wettability and boiling heat transfer study of black silicon surface produced using the plasma immersion ion implantation method.* Applied Thermal Engineering, 2016. **99**: p. 253-261.

25.   Kweon, Y. and M. Kim, *Experimental study on nucleate boiling enhancement and bubble dynamic behavior in saturated pool boiling using a nonuniform dc electric field.* International Journal of Multiphase Flow, 2000. **26**(8): p. 1351-1368.

26.   Mukherjee, A. and S.G. Kandlikar, *Numerical study of single bubbles with dynamic contact angle during nucleate pool boiling.* International Journal of Heat and Mass Transfer, 2007. **50**(1): p. 127-138.

27.   Hsieh, S.-S. and C.-G. Ke, *Bubble dynamic parameters and pool boiling heat transfer on plasma coated tubes in saturated R-134a and R-600a.* Journal of HeatTransfer, 2002. **124**(4): p. 704-716.

28.   Barthau, G., *Active nucleation site density and pool boiling heat transfer—an experimental study.* International Journal of Heat and Mass Transfer, 1992. **35**(2): p. 271-278.

29.   Benjamin, R. and A. Balakrishnan, *Nucleation site density in pool boiling of saturated pure liquids: effect of surface microroughness and surface and liquid physical properties.* Experimental Thermal and Fluid Science, 1997. **15**(1): p. 32-42.

30.   Yang, S. and R. Kim, *A mathematical model of the pool boiling nucleation site density in terms of the surface characteristics.* International Journal of Heat and MassTransfer, 1988. **31**(6): p. 1127-1135.

31.   Wang, C. and V. Dhir, *Effect of surface wettability on active nucleation site density during pool boiling of water on a vertical surface.* Journal of Heat Transfer, 1993. **115**(3): p. 659-669.

32.   Sarafraz, M., F. Hormozi and S. Peyghambarzadeh, *Pool boiling heat transfer to aqueous alumina nano-fluids on the plain and concentric circular micro-structured (CCM) surfaces.* Experimental Thermal and Fluid Science, 2016. **72**: p. 125-139.

33.   Kim, S., H.D. Kim, H. Kim, H.S. Ahn, H. Jo, J. Kim and M.H. Kim, *Effects of nano-fluid and surfaces with nano structure on the increase of CHF.* Experimental Thermal and Fluid Science, 2010. **34**(4): p. 487-495.

34.   Ahn, H.S. and M.H. Kim, *A review on critical heat flux enhancement with nanofluids and surface modification.* Journal of Heat Transfer, 2012. **134**(2): p. 024001.

35.   Tang, Y., B. Tang, Q. Li, J. Qing, L. Lu and K. Chen, *Pool-boiling enhancement by novel metallic nanoporous surface.* Experimental Thermal and Fluid Science, 2013. **44**: p. 194-198.

36.   Mao, R., S. Liang, X. Wang, Q. Yang and B. Han, *Effect of preparation conditions on morphology and thermal stability of nanoporous copper.* Corrosion Science, 2012. **60**: p. 231-237.

37. Hayes, J., A. Hodge, J. Biener, A. Hamza and K. Sieradzki, *Monolithic nanoporous copper by dealloying Mn–Cu.* Journal of Materials Research, 2006. **21**(10): p. 2611-2616.

38. Zhang, Z., Y. Wang, Z. Qi, J. Lin and X. Bian, *Nanoporous gold ribbons with bimodal channel size distributions by chemical dealloying of Al− Au alloys.* The Journal of Physical Chemistry C, 2009. **113**(4): p. 1308-1314.

39. Zhao, C., Z. Qi, X. Wang and Z. Zhang, *Fabrication and characterization of monolithic nanoporous copper through chemical dealloying of Mg–Cu alloys.* Corrosion Science, 2009. **51**(9): p. 2120-2125.

40. Xu, P., Q. Li and Y. Xuan, *Enhanced boiling heat transfer on composite porous surface.* International Journal of Heat and Mass Transfer, 2015. **80**: p. 107-114.

41. Lee, C.Y., M.M.H. Bhuiya and K.J. Kim, *Pool boiling heat transfer with nano-porous surface.* International Journal of Heat and Mass Transfer, 2010. **53**(19-20): p. 4274-4279.

42. Li, C.H., T. Li, P. Hodgins, C.N. Hunter, A.A. Voevodin, J.G. Jones and G.P. Peterson, *Comparison study of liquid replenishing impacts on critical heat flux and heat transfer coefficient of nucleate pool boiling on multiscale modulated porous structures.* International Journal of Heat and Mass Transfer, 2011. **54**(15-16): p. 3146-3155.

43. Tang, Y., B. Tang, Q. Li, J.B. Qing, L.S. Lu and K.P. Chen, *Pool-boiling enhancement by novel metallic nanoporous surface.* Experimental Thermal and Fluid Science, 2013. **44**: p. 194-198.

44. Deng, D., W. Wan, J. Feng, Q. Huang, Y. Qin and Y. Xie, *Comparative experimental study on pool boiling performance of porous coating and solid structures with reentrant channels.* Applied Thermal Engineering, 2016. **107**: p. 420-430.

45. Deng, D., J. Feng, Q. Huang, Y. Tang and Y. Lian, *Pool boiling heat transfer of porous structures with reentrant cavities.* International Journal of Heat and Mass Transfer, 2016. **99**: p. 556-568.

46. Ramilison, J.M. and J. Lienhard, *Transition boiling heat transfer and the film transition regime.* Journal of Heat Transfer, 1987. **109**(3): p. 746-752.

47. Haramura, Y. *Steady state pool transition boiling heated with condensing steam.* in *Proc. ASME/JSME Thermal Engineering Joint Conf.* 1991.

48. Liaw, S.-P. and V. Dhir. *Effect of surface wettability on transition boiling heat transfer from a vertical surface.* in *Proceedings of the 8th International Heat Transfer Conference.* 1986.

49. Maracy, M. and R. Winterton, *Hysteresis and contact angle effects in transition pool boiling of water.* International Journal of Heat and Mass Transfer, 1988. **31**(7): p. 1443-1449.

50. Sadaghiani, A.K., A. Motezakker, A.V. Ozpinar, G. Ozaydin-Ince and A. Kosar, *Pool boiling heat transfer characteristics of inclined pHEMA (polyhydroxyethylmethacrylate) coated surfaces.* Journal of Heat Transfer.

51. Ahn, H.S., C. Lee, H. Kim, H. Jo, S. Kang, J. Kim, J. Shin and M.H. Kim, *Pool boiling CHF enhancement by micro/nanoscale modification of zircaloy-4 surface.* Nuclear Engineering and Design, 2010. **240**(10): p. 3350-3360.

52. Kandlikar, S., *Controlling bubble motion over heated surface through evaporation momentum force to enhance pool boiling heat transfer.* Applied Physics Letters, 2013. **102**(5): p. 051611.

53. Dhillon, N.S., J. Buongiorno and K.K. Varanasi, *Critical heat flux maxima during boiling crisis on textured surfaces.* Nature communications, 2015. **6**.

54. Zou, A. and S.C. Maroo, *Critical height of micro/nano structures for pool boiling heat transfer enhancement.* Applied Physics Letters, 2013. **103**(22): p. 221602.

55. Sarangi, S., J.A. Weibel and S.V. Garimella, *Effect of particle size on surface-coating enhancement of pool boiling heat transfer.* International Journal of Heat and Mass Transfer, 2015. **81**: p. 103-113.

56. Hsu, C.-C. and P.-H. Chen, *Surface wettability effects on critical heat flux of boiling heat transfer using nanoparticle coatings.* International Journal of Heat and Mass Transfer, 2012. **55**(13): p. 3713-3719.

57. Yao, Z., Y.-W. Lu and S.G. Kandlikar, *Fabrication of nanowires on orthogonal surfaces of microchannels and their effect on pool boiling.* Journal of Micromechanics and Microengineering, 2012. **22**(11): p. 115005.

58. Chen, R., M.-C. Lu, V. Srinivasan, Z. Wang, H.H. Cho and A. Majumdar, *Nanowires for enhanced boiling heat transfer.* Nano letters, 2009. **9**(2): p. 548-553.

59. Li, D., G. Wu, W. Wang, Y. Wang, D. Liu, D. Zhang, Y. Chen, G. Peterson and R. Yang, *Enhancing flow boiling heat transfer in microchannels for thermal management with monolithically-integrated silicon nanowires.* Nano letters, 2012. **12**(7): p. 3385-3390.

60. Ahn, H.S., C. Lee, J. Kim and M.H. Kim, *The effect of capillary wicking action of micro/nano structures on pool boiling critical heat flux.* International Journal of Heat and Mass Transfer, 2012. **55**(1): p. 89-92.

61. Patil, C.M. and S.G. Kandlikar, *Review of the manufacturing techniques for porous surfaces used in enhanced pool boiling.* Heat Transfer Engineering, 2014. **35**(10): p. 887-902.

62. Ahn, H.S., J.M. Kim, C. Park, J.-W. Jang, J.S. Lee, H. Kim, M. Kaviany and M.H. Kim, *A Novel Role of Three Dimensional Graphene Foam to Prevent Heater Failure during Boiling.* Scientific Reports, 2013. **3**: p. 1960.

63. Novoselov, K., D. Jiang, F. Schedin, T. Booth, V. Khotkevich, S. Morozov and A. Geim, *Two-dimensional atomic crystals.* Proceedings of the National Academy of Sciences of the United States of America, 2005. **102**(30): p. 10451-10453.

64. Neto, A.C., F. Guinea, N.M. Peres, K.S. Novoselov and A.K. Geim, *The electronic properties of graphene.* Reviews of modern physics, 2009. **81**(1): p. 109.

65. Scarpa, F., S. Adhikari and A.S. Phani, *Effective elastic mechanical properties of single layer graphene sheets.* Nanotechnology, 2009. **20**(6): p. 065709.

66. Bonaccorso, F., Z. Sun, T. Hasan and A. Ferrari, *Graphene photonics and optoelectronics.* Nature photonics, 2010. **4**(9): p. 611-622.

67. Yavari, F., Z. Chen, A.V. Thomas, W. Ren, H.-M. Cheng and N. Koratkar, *High sensitivity gas detection using a macroscopic three-dimensional graphene foam network.* Scientific reports, 2011. **1**.

68. Fang, Q., Y. Shen and B. Chen, *Synthesis, decoration and properties of three-dimensional graphene-based macrostructures: a review.* Chemical Engineering Journal, 2015. **264**: p. 753-771.

69. Mao, S., G. Lu and J. Chen, *Three-dimensional graphene-based composites for energy applications.* Nanoscale, 2015. **7**(16): p. 6924-6943.

70. Zhang, L. and G. Shi, *Preparation of highly conductive graphene hydrogels for fabricating supercapacitors with high rate capability.* The Journal of Physical Chemistry C, 2011. **115**(34): p. 17206-17212.

71. Xue, Y., D. Yu, L. Dai, R. Wang, D. Li, A. Roy, F. Lu, H. Chen, Y. Liu and J. Qu, *Three-dimensional B, N-doped graphene foam as a metal-free catalyst for oxygen reduction reaction.* Physical Chemistry Chemical Physics, 2013. **15**(29): p. 12220-12226.

72. Lee, J.-S., H.-J. Ahn, J.-C. Yoon and J.-H. Jang, *Three-dimensional nano-foam of few-layer graphene grown by CVD for DSSC.* Physical Chemistry Chemical Physics, 2012. **14**(22): p. 7938-7943.

73. Zhang, X., Z. Sui, B. Xu, S. Yue, Y. Luo, W. Zhan and B. Liu, *Mechanically strong and highly conductive graphene aerogel and its use as electrodes for electrochemical power sources.* Journal of Materials Chemistry, 2011. **21**(18): p. 6494-6497.

74. Yong, Y.-C., X.-C. Dong, M.B. Chan-Park, H. Song and P. Chen, *Macroporous and monolithic anode based on polyaniline hybridized three-dimensional graphene for high-performance microbial fuel cells.* ACS nano, 2012. **6**(3): p. 2394-2400.

75. Cao, X., Y. Shi, W. Shi, G. Lu, X. Huang, Q. Yan, Q. Zhang and H. Zhang, *Preparation of novel 3D graphene networks for supercapacitor applications.* Small, 2011. **7**(22): p. 3163-3168.

76. Pettes, M.T., H. Ji, R.S. Ruoff and L. Shi, *Thermal transport in three-dimensional foam architectures of few-layer graphene and ultrathin graphite.* Nano letters, 2012. **12**(6): p. 2959-2964.

77. Lin, H., S. Xu, X. Wang and N. Mei, *Significantly reduced thermal diffusivity of free-standing two-layer graphene in graphene foam.* Nanotechnology, 2013. **24**(41): p. 415706.

78. Nguyen, D.D., N.-H. Tai, S.-B. Lee and W.-S. Kuo, *Superhydrophobic and superoleophilic properties of graphene-based sponges fabricated using a facile dip coating method.* Energy & Environmental Science, 2012. **5**(7): p. 7908-7912.

79. Dong, X., Y. Cao, J. Wang, M.B. Chan-Park, L. Wang, W. Huang and P. Chen, *Hybrid structure of zinc oxide nanorods and three dimensional graphene foam for supercapacitor and electrochemical sensor applications.* RSC Advances, 2012. **2**(10): p. 4364-4369.

80. Tetreault-Friend, M., R. Azizian, M. Bucci, T. McKrell, J. Buongiorno, M. Rubner and R. Cohen, *Critical heat flux maxima resulting from the controlled morphology of nanoporous hydrophilic surface layers.* Applied Physics Letters, 2016. **108**(24): p. 243102.

81. Chang, J. and S. You, *Enhanced boiling heat transfer from microporous surfaces: effects of a coating composition and method.* International Journal of Heat and Mass Transfer, 1997. **40**(18): p. 4449-4460.

82. Liter, S.G. and M. Kaviany, *CHF enhancement by modulated porous-layer coating.* ASME HEAT TRANSFER DIV PUBL HTD, 1998. **361**: p. 165-173.

83. Li, C. and G. Peterson, *Experimental study of enhanced nucleate boiling heat transfer on uniform and modulated porous structures.* Frontiers in Heat and Mass Transfer (FHMT), 2010. **1**(2).

84. Coleman, H.W. and W.G. Steele, *Experimentation, validation, and uncertainty analysis for engineers.* 2009: John Wiley & Sons.

85. Rayleigh, L., *VIII. On the pressure developed in a liquid during the collapse of a spherical cavity.* The London, Edinburgh, and Dublin Philosophical Magazine and Journal of Science, 1917. **34**(200): p. 94-98.

86. Mikic, B., W. Rohsenow and P. Griffith, *On bubble growth rates.* International Journal of Heat and Mass Transfer, 1970. **13**(4): p. 657-666.

87. McHale, J.P. and S.V. Garimella, *Bubble nucleation characteristics in pool boiling of a wetting liquid on smooth and rough surfaces.* International Journal of Multiphase Flow, 2010. **36**(4): p. 249-260.

88.	Michaelides, E.E., *Hydrodynamic force and heat/mass transfer from particles, bubbles, and drops—the Freeman scholar lecture.* Journal of Fluids Engineering, 2003. **125**(2): p. 209-238.

89.	Ishii, M. and N. Zuber, *Drag coefficient and relative velocity in bubbly, droplet or particulate flows.* AIChE Journal, 1979. **25**(5): p. 843-855.

90.	DeLong, E.F., *Everything in moderation: archaea as 'non-extremophiles'.* Current Opinion in Genetics & Development, 1998. **8**(6): p. 649-654.

91.	Reeve, J.N., *Archaebacteria then… Archaes now (are there really no archaeal pathogens?).* Journal of Bacteriology, 1999. **181**(12): p. 3613-3617.

92.	Woese, C.R. and G.E. Fox, *Phylogenetic structure of the prokaryotic domain: the primary kingdoms.* Proceedings of the National Academy of Sciences, 1977. **74**(11): p. 5088-5090.

93.	Ciaramella, M., F.M. Pisani and M. Rossi, *Molecular biology of extremophiles: recent progress on the hyperthermophilic archaeon Sulfolobus.* Antonie Van Leeuwenhoek, 2002. **81**(1-4): p. 85-97.

94.	Bell, S.D. and S.P. Jackson, *Transcription and translation in Archaea: a mosaic of eukaryal and bacterial features.* Trends in Microbiology, 1998. **6**(6): p. 222-228.

95.	Chaban, B., S.Y. Ng and K.F. Jarrell, *Archaeal habitats—from the extreme to the ordinary.* Canadian Journal of Microbiology, 2006. **52**(2): p. 73-116.

96.	Schleper, C., G. Puehler, I. Holz, A. Gambacorta, D. Janekovic, U. Santarius, H.-P. Klenk and W. Zillig, *Picrophilus gen. nov., fam. nov.: a novel aerobic, heterotrophic, thermoacidophilic genus and family comprising archaea capable of growth around pH 0.* Journal of Bacteriology, 1995. **177**(24): p. 7050-7059.

97.	Kashefi, K. and D.R. Lovley, *Extending the upper temperature limit for life.* Science, 2003. **301**(5635): p. 934-934.

98.	Moll, R. and G. Schäfer, *Chemiosmotic H+ cycling across the plasma membrane of the thermoacidophilic archaebacterium Sulfolobus acidocaldarius.* FEBS Letters, 1988. **232**(2): p. 359-363.

99.	Grogan, D.W., *Phenotypic characterization of the archaebacterial genus Sulfolobus: comparison of five wild-type strains.* Journal of Bacteriology, 1989. **171**(12): p. 6710-6719.

100.	Brock, T.D., K.M. Brock, R.T. Belly and R.L. Weiss, *Sulfolobus: a new genus of sulfur-oxidizing bacteria living at low pH and high temperature.* Archives of Microbiology, 1972. **84**(1): p. 54-68.

101.	Singh, S.K., S. Khandekar, D. Pratap and S.A. Ramakrishna, *Wetting dynamics and evaporation of sessile droplets on nano-porous alumina surfaces.* Colloids and Surfaces A: Physicochemical and Engineering Aspects, 2013. **432**: p. 71-81.

102. Das, S. and S. Bhaumik, *Experimental study of nucleate pool boiling heat transfer using water on thin-film surface.* Iranian Journal of Science and Technology, Transactions of Mechanical Engineering, 2016. **40**(1): p. 21-29.

103. Schrenk, M.O., D.S. Kelley, S.A. Bolton and J.A. Baross, *Low archaeal diversity linked to subseafloor geochemical processes at the Lost City Hydrothermal Field, Mid-Atlantic Ridge.* Environmental Microbiology, 2004. **6**(10): p. 1086-1095.

104. Macalady, J.L., D.S. Jones and E.H. Lyon, *Extremely acidic, pendulous cave wall biofilms from the Frasassi cave system, Italy.* Environmental Microbiology, 2007. **9**(6): p. 1402-1414.

105. Niederberger, T.D., D.K. Götz, I.R. McDonald, R.S. Ronimus and H.W. Morgan, *Ignisphaera aggregans gen. nov., sp. nov., a novel hyperthermophilic crenarchaeote isolated from hot springs in Rotorua and Tokaanu, New Zealand.* International Journal of Systematic and Evolutionary Microbiology, 2006. **56**(5): p. 965-971.

106. Ionescu, D., C. Siebert, L. Polerecky, Y.Y. Munwes, C. Lott, S. Häusler, M. Bižić-Ionescu, C. Quast, J. Peplies and F.O. Glöckner, *Microbial and chemical characterization of underwater fresh water springs in the Dead Sea.* PloS one, 2012. **7**(6): p. e38319.

107. Davey, M.E. and G.A. O'toole, *Microbial biofilms: from ecology to molecular genetics.* Microbiology and Molecular Biology Reviews, 2000. **64**(4): p. 847-867.

108. Flemming, H.-C. and J. Wingender, *The biofilm matrix.* Nature Reviews. Microbiology, 2010. **8**(9): p. 623.

109. Zolghadr, B., A. Klingl, A. Koerdt, A.J. Driessen, R. Rachel and S.-V. Albers, *Appendage-mediated surface adherence of Sulfolobus solfataricus.* Journal of Bacteriology, 2010. **192**(1): p. 104-110.

110. Schrenk, M.O., D.S. Kelley, J.R. Delaney and J.A. Baross, *Incidence and diversity of microorganisms within the walls of an active deep-sea sulfide chimney.* Applied and Environmental Microbiology, 2003. **69**(6): p. 3580-3592.

111. Henche, A.L., A. Koerdt, A. Ghosh and S.V. Albers, *Influence of cell surface structures on crenarchaeal biofilm formation using a thermostable green fluorescent protein.* Environmental Microbiology, 2012. **14**(3): p. 779-793.

112. Fröls, S., M. Ajon, M. Wagner, D. Teichmann, B. Zolghadr, M. Folea, E.J. Boekema, A.J. Driessen, C. Schleper and S.V. Albers, *UV-inducible cellular aggregation of the hyperthermophilic archaeon Sulfolobus solfataricus is mediated by pili formation.* Molecular Microbiology, 2008. **70**(4): p. 938-952.

113. Koerdt, A., S. Jachlewski, A. Ghosh, J. Wingender, B. Siebers and S.-V. Albers, *Complementation of Sulfolobus solfataricus PBL2025 with an α-mannosidase: effects on surface attachment and biofilm formation.* Extremophiles, 2012. **16**(1): p. 115-125.

114. Ajon, M., S. Fröls, M. van Wolferen, K. Stoecker, D. Teichmann, A.J. Driessen, D.W. Grogan, S.V. Albers and C. Schleper, *UV-inducible DNA exchange in hyperthermophilic archaea mediated by type IV pili.* Molecular Microbiology, 2011. **82**(4): p. 807-817.

115. Furberg, R., B. Palm, S. Li, M. Toprak and M. Muhammed, *The use of a nano-and microporous surface layer to enhance boiling in a plate heat exchanger.* Journal of Heat Transfer, 2009. **131**(10): p. 101010.

116. Liter, S.G. and M. Kaviany, *Pool-boiling CHF enhancement by modulated porous-layer coating: theory and experiment.* International Journal of Heat and Mass Transfer, 2001. **44**(22): p. 4287-4311.

117. Ha, M. and S. Graham. *Pool boiling enhancement through hierarchical texturing of surfaces.* in *Thermal and Thermomechanical Phenomena in Electronic Systems (ITherm), 2016 15th IEEE Intersociety Conference on.* 2016. IEEE.

118. Huh, C. and L. Scriven, *Hydrodynamic model of steady movement of a solid/liquid/fluid contact line.* Journal of Colloid and Interface Science, 1971. **35**(1): p. 85-101.

119. Nikolayev, V.S., *Dynamics of the triple contact line on a nonisothermal heater at partial wetting.* Physics of Fluids, 2010. **22**(8): p. 082105.

120. Choi, C. and M. Kim, *Wettability effects on heat transfer*, in *Two Phase Flow, Phase Change and Numerical Modeling.* 2011, InTech.

121. Vinogradova, O., N. Bunkin, N. Churaev, O. Kiseleva, A. Lobeyev and B. Ninham, *Submicrocavity structure of water between hydrophobic and hydrophilic walls as revealed by optical cavitation.* Journal of Colloid and Interface Science, 1995. **173**(2): p. 443-447.

122. Betz, A.R., J. Xu, H. Qiu and D. Attinger, *Do surfaces with mixed hydrophilic and hydrophobic areas enhance pool boiling.* Applied Physics Letters, 2010. **97**(14): p. 141909.

123. Betz, A.R., J. Jenkins and D. Attinger, *Boiling heat transfer on superhydrophilic, superhydrophobic, and superbiphilic surfaces.* International Journal of Heat and Mass Transfer, 2013. **57**(2): p. 733-741.

124. Jansen, H., M. de Boer, R. Legtenberg and M. Elwenspoek, *The black silicon method: a universal method for determining the parameter setting of a fluorine-based reactive ion etcher in deep silicon trench etching with profile control.* Journal of Micromechanics and Microengineering, 1995. **5**(2): p. 115.

125. Schmidt, M.S., J. Hübner and A. Boisen, *Large area fabrication of leaning silicon nanopillars for surface enhanced Raman spectroscopy.* Advanced Materials, 2012. **24**(10).

126. Hsu, C.-M., S.T. Connor, M.X. Tang and Y. Cui, *Wafer-scale silicon nanopillars and nanocones by Langmuir–Blodgett assembly and etching.* Applied Physics Letters, 2008. **93**(13): p. 133109.

127. Wierzbicki, R., M.S. Schmidt, A. Boisen, D. Engstrøm, K. Mølhave and P. Bøggild, *Black silicon maskless templates for carbon nanotube forests.* Microelectronic Engineering, 2013. **104**: p. 110-113.

128. Jo, H., H.S. Ahn, S. Kang and M.H. Kim, *A study of nucleate boiling heat transfer on hydrophilic, hydrophobic and heterogeneous wetting surfaces.* International Journal of Heat and Mass Transfer, 2011. **54**(25-26): p. 5643-5652.

129. Phan, H.T., N. Caney, P. Marty, S. Colasson and J. Gavillet, *Surface wettability control by nanocoating: the effects on pool boiling heat transfer and nucleation mechanism.* International Journal of Heat and Mass Transfer, 2009. **52**(23-24): p. 5459-5471.

130. Mikic, B. and W. Rohsenow, *A new correlation of pool-boiling data including the effect of heating surface characteristics.* Journal of Heat Transfer, 1969. **91**(2): p. 245-250.

131. Gong, S. and P. Cheng, *Numerical simulation of pool boiling heat transfer on smooth surfaces with mixed wettability by lattice Boltzmann method.* International Journal of Heat and Mass Transfer, 2015. **80**: p. 206-216.